ISTANBUL TECHNICAL UNIVERSITY ★ GRADUATE SCHOOL

UTILIZATION OF CARBON DIOXIDE GAS FOR GAS LIFT SYSTEMS IN GEOTHERMAL WELLS

M.Sc. THESIS

Force Lugembe NDEGE

Department of Petroleum and Natural Gas Engineering

Petroleum and Natural Gas Engineering Programme

AUGUST 2025

ISTANBUL TECHNICAL UNIVERSITY ★ GRADUATE SCHOOL

UTILIZATION OF CARBON DIOXIDE GAS FOR GAS LIFT SYSTEMS IN GEOTHERMAL WELLS

M.Sc. THESIS

Force Lugembe NDEGE
(505211505)

Department of Petroleum and Natural Gas Engineering

Petroleum and Natural Gas Engineering Programme

Thesis Advisor: Prof. Dr. Ömer İnanç TÜREYEN

AUGUST 2025

İSTANBUL TEKNİK ÜNİVERSİTESİ ★ LİSANSÜSTÜ EĞİTİM ENSTİTÜSÜ

JEOTERMAL KUYULARDA GAZ KALDIRMA SİSTEMLERİ İÇİN KARBON DİOKSİT GAZININ KULLANIMI

YÜKSEK LİSANS TEZİ

Force Lugembe NDEGE
(505211505)

Petrol ve Doğal Gaz Mühendisliği Anabilim Dalı

Petrol ve Doğal Gaz Mühendisliği Programı

Tez Danışmanı: Prof. Dr. Ömer İnanç TÜREYEN

AĞUSTOS 2025

Force Lugembe NDEGE, a M.Sc. student of İTU Graduate School student ID 505211505, successfully defended the thesis entitled “UTILIZATION OF CARBON DIOXIDE GAS FOR GAS LIFT SYSTEMS IN GEOTHERMAL WELLS”, which he prepared after fulfilling the requirements specified in the associated legislations, before the jury whose signatures are below.

Thesis Advisor : **Prof. Dr. Ömer İnanç TÜREYEN** .....
Istanbul Technical University

Jury Members : **Asst. Prof. Dr. Emine Didem KORKMAZ BAŞEL** .....
Istanbul Technical University

Assoc. Prof. Dr. İsmail DURGUT .....
Middle East Technical University

Date of Submission : 29 July 2025
Date of Defense : 06 August 2025

To The Memory of My Loving Grandmother Silya NDUTI,

FOREWORD

Firstly, I would want to thank Presidency for Turks Abroad and Related Communities (YTB) for their financial support during my master's degree study at Istanbul Technical University; it was an honour to be one of the YTB scholarship recipient.

Secondly, I would like to express my sincere gratitude to my advisor, Prof. Dr. Ömer İnanç TÜREYEN, for his valuable guidance, insightful advice, and patience throughout the course of the Thesis work. His support has been important to my academic journey, and I will always carry with me the knowledge and experience gained under his supervision, even as I pursue future career paths.

I would also like to express my sincere appreciation to the faculty members of the Petroleum and Natural Gas Engineering Department at Istanbul Technical University, including Prof. Dr. Abdurrahman SATMAN, Asst. Prof. Dr. Emine Didem KORKMAZ BAŞEL, Dr. Lect. Yıldıray PALABIYIK, Assoc. Prof. Dr. Hasan Ozgur YILDIZ, Prof. Dr. Gurşat ALTUN, and Assist. Prof. Metin MIHÇAKAN for their academic support.

I am especially grateful to my friends Dr. Hanane ELNAGDY, Dr. Sarah Yaseen ABDULRAZZAQ, Nariman VALİYEV Md Anwar Hossen for their motivation and support, which helped me stay motivated and focused.

Finally, I would like to thank my mother who provided emotional strength and helped me remain grounded throughout this journey.

August 2025

Force Lugembe NDEGE
(Petroleum and Natural Gas Engineer, M.Sc.)

TABLE OF CONTENTS

Page

FOREWORD ..... **ix**
TABLE OF CONTENTS ..... **xi**
ABBREVIATIONS ..... **xiii**
LIST OF SYMBOLS ..... **xv**
LIST OF TABLES ..... **xvii**
LIST OF FIGURES ..... **xix**
SUMMARY ..... **xxi**
ÖZET ..... **xxiii**
1. INTRODUCTION **1**
2. LITERATURE REVIEW ON GEOTHERMAL WELLBORE MODELLING **5**
3. STATEMENT OF THE PROBLEM **9**
4. METHODOLOGY **11**
4.1 Duan's CO_2 Solubility Model 11
4.2 Well Pressure Profile Model 12
4.3 Implementation 12
5. DUAN MODEL **13**
5.1 Description of the Model 13
5.2 Model Against Model Validation of The CO2 Solubility Code 13
5.3 Model Against Experimental Data Validation of the CO2 Solubility Code 14
6. FLASH POINT PRESSURE AND CO_2 MASS FRACTIONS RELATIONSHIP **17**
7. WELL PRESSURE PROFILE MODEL **19**
7.1 Numerical Model Execution 20
7.2 Validation of the Well Model 21
7.2.1 Validation of the model to the AF-21 well 21
7.2.2 Data acquisition and digitization 21
7.3 Validation of the Model to the OB-16 Well 22
7.3.1 Data acquisition and digitization 23
7.4 Validation of the Model to the K-49 Well 23
8. DETAILS OF THE MODEL USED IN THIS STUDY **25**
8.1 Description of the Code 25
8.2 Equations of Pressure and Temperature Used for The Code 26
8.2.1 Single phase flow 26
8.2.2 The study on the flash point pressure in a wellbore 28
8.2.3 Double phase flow 28
9. RESULTS AND DISCUSION **31**
9.1 Sensitivity Analysis 31
9.1.1 Influence of varying co_2 mass fractions on flash point pressure and depth 32

9.1.2 Influence of varying co_2 mass fractions and flow rates on wellhead pressure 33
10. INFLUENCE OF VARYING CO_2 MASS FRACTIONS ON GEOTHERMAL FLUID DENSITY 35
11. CONCLUSION 37
REFERENCES 39
APPENDIX 43
CURRICULUM VITAE 55

ABBREVIATIONS

bh	**:** Bottom hole
CO_2	**:** Carbon dioxide
ei	**:** Ambient
g	**:** Gas
i	**:** Initial
L	**:** Liquid
m	**:** Mixture
sg	**:** Gas phase superficial
tr	**:** Terminal
w	**:** Water
wf	**:** Bottom hole flowing fluid

LIST OF SYMBOLS

a	**:** Geothermal gradient, ºF / ft
A'	**:** Diffusion depth, ft
c	**:** Specific heat capacity, Btu/lbm -°F
d	**:** Diameter, ft
dL	**:** Segment length, ft
f	**:** Moody friction factor
f_g	**:** Gas holdup (void fraction)
f_L	**:** Liquid hold-up (liquid hold up)
f(t)	**:** Dimensionless time function
g	**:** Gravitational acceleration, m / s2
gc	**:** Unit conversion factor, 32.17 (lbm - ft) / lbf / s2
ke	**:** Thermal conductivity of formation, (Btu/ft-day-°F)
m	**:** Mass, kg
P	**:** Pressure, bar
q	**:** Flow rate, ft3 / s
r2'	**:** Outer radius, ft
t	**:** Time, day
tD	**:** Dimensionless time
T	**:** Temperature, °F
w	**:** Mass flow rate, lbm / h
x	**:** Mass ratio
y	**:** Gas mass fraction in the gas phase
X	**:** Gas mass fraction in the liquid phase
a	**:** Thermal diffusivity of the formation (thermal diffusivity), (ft2/day)
ρ	**:** Density, lbm/ft3
μ	**:** Viscosity, cp
v	**:** Fluid velocity, ft / s

LIST OF TABLES

Page

Table 7.1 : The input parameters of the A-21 well. **21**

LIST OF FIGURES

Page

Figure 5.1 : Modeling Solubility data of CO_2 in water under various temperature and pressure conditions by Duan (2003). **13**
Figure 5.2 : Comparison between Duan's CO_2 solubility data and code calculated CO_2 solubility in water from 273.15K to 533.15K and pressures up to 900bar..... **14**
Figure 5.3 : A comparison of CO_2 solubility between the code calculated values in this study and those published in the literature at 40^0C (A) and 50^0C (B) respectively. The solid lines represent the solubility values calculated by using Duan's model. **15**
Figure 6.1 : Effect of changing mass fractions to flash point pressure. **17**
Figure 7.1 : Pressure-depth profile illustrating flash point depth and pressure in a geothermal well..... **20**
Figure 7.2 : The pressure profile of the AF-21 well and the model, where the mass fraction of the dissolve CO_2 is at 0.9%. **22**
Figure 7.3 : The pressure profile of the OB-16 well and the model, where the mass fraction of the dissolved CO_2 is at 3.21%. **23**
Figure 7.4 : Comparison between code model computed and K-49 measured pressure profile. **24**
Figure 8.1 : Flowchart for computing the wellbore pressure profile. **26**
Figure 9.1 : Results of the pressure profile of the OB-16 well with various CO_2 mass fractions. **32**
Figure 9.2 : Results of the pressure profile of the K-49 well with various CO_2 mass fractions. **33**
Figure 9.3 : Results of flash point depth with various CO_2 mass fractions. **33**
Figure 9.4 : Results of wellhead pressure with various CO_2 mass fractions and flow rates. **34**
Figure 10.1 : Results of Influence of varying CO_2 mass fractions on Fluid Density.**36**

UTILIZATION OF CARBON DIOXIDE GAS FOR GAS LIFT SYSTEMS IN GEOTHERMAL WELLS

SUMMARY

Geothermal wells experience a decline in pressure between the bottomhole pressure and the wellhead pressure (during both static and dynamic conditions) due to friction and gravity. In some cases, this decline could be large, leading to reduced production rates. High wellhead pressures are necessary for maintaining high production rates and keeping the geothermal power plants operational. To address the pressure loss during fluid flow in geothermal wells, artificial lift techniques are employed, such as line shaft pumps and electrical submersible pumps (ESPs), which are widely used in Türkiye and globally.

This study investigates the feasibility and potential benefits of using carbon dioxide gas lift systems in geothermal wells as an innovative artificial lift technique. The utilization of CO_2 gas for gas lift in geothermal wells, though not widely researched and adopted, presents a promising approach to enhancing the productivity and efficiency of geothermal energy extraction. By integrating CO_2 gas lift systems, operators can improve flow rates, increase overall system efficiency, and reduce operational costs.

The study involves several stages, including the analysis of the thermodynamic behavior and solubility of CO_2 in water at various pressures and temperatures encountered during geothermal fluid flow. Using Duan's solubility data, the solubility of CO_2 in water was predicted with high accuracy through python coding techniques, covering pressures up to 2000 bar and temperatures of 533K. Additionally, geothermal pressure profiles, partial pressures of steam and CO_2, and flash point pressures were simulated by python coding and validated, to understand the effects of varying CO_2 mass fractions. It was discovered that increasing CO_2 mass fractions reduced pressure losses, leading to higher wellhead pressures.

This study's findings indicate that CO_2 has a profound effect on the wellhead pressure. Therefore, CO_2 gas lift systems may serve as a viable alternative to conventional artificial lift techniques. By addressing challenges such as declining productivity and operational inefficiencies, the integration of CO_2 gas lift systems contributes to improved energy production and lower operational costs. This research provides a comprehensive understanding of the effects of CO_2 on the production performance for geothermal wells.

JEOTERMAL KUYULARDA GAZ KALDIRMA SİSTEMLERİ İÇİN KARBON DİOKSİT GAZININ KULLANIMI

ÖZET

Jeotermal kuyularda, doğal ve işletme koşullarına bağlı olarak, kuyu tabanı basıncı ile kuyu başı basıncı arasında hem statik hem de dinamik durumlarda basınç kayıpları meydana gelir. Bu kayıpların en önemli nedenlerinden biri, kuyu içindeki akışkanın yükselişi sırasında ortaya çıkan yerçekimi kaynaklı hidrolik yük ve sürtünme kayıplarıdır. Jeotermal akışkanın kuyu tabanından yüzeye taşınması sırasında yoğunluk, viskoz sürtünme ve faz değişimi etkilerinin birleşimi basınçta belirgin düşüşlere yol açar. Bu düşüş belirli bir seviyenin üzerine çıktığında, üretim debisi azalır ve santral kapasitesi düşer. Hatta bazı durumlarda, kuyu herhangi bir müdahale yapılmaksızın üretimi sürdüremeyebilir.

Dolayısıyla, yeterli kuyu başı basıncının korunması, jeotermal santrallerin tasarım kapasitelerine yakın çalışabilmesi için kritik öneme sahiptir. Klasik yapay kaldırma yöntemleri, düşey milli pompalar (LSP) veya elektrikli daldırma pompaları (ESP) gibi çözümlere dayanır. Ancak bu pompalar yüksek sıcaklık ve yüksek entalpiye sahip jeotermal ortamlarda; termal bozulma, mekanik aşınma, korozyon ve kireçlenme gibi ciddi problemlerle karşılaşır. Derin veya eğimli kuyularda kurulum ve bakım işlemleri teknik açıdan güç, maliyet açısından da yüksek olmaktadır. Ayrıca, pompaların yüksek enerji tüketimi, santral verimliliğini azaltarak jeotermal enerjinin çevresel ve ekonomik avantajlarını gölgeleyebilmektedir.

Bu zorluklara alternatif olarak, bu çalışmada petrol endüstrisinde yaygın kullanılan ancak jeotermal uygulamalarda büyük ölçüde araştırılmamış olan CO_2 gaz kaldırma sistemleri incelenmiştir. Gaz kaldırma yöntemi, belirli derinliklere yerleştirilen valfler aracılığıyla üretim borusu içerisine gaz enjekte edilmesi prensibine dayanır. Enjekte edilen gaz sıvı kolonunun yoğunluğunu azaltarak hidrostatik basıncı düşürür ve böylece akışkanın yüzeye çıkışı kolaylaşır. Bazı jeotermal sahalarda azot (N_2) gazı bu amaçla kullanılmış olsa da, jeotermal rezervuarlarda doğal olarak yüksek miktarlarda bulunan CO_2 gazı, entegre ve sürdürülebilir bir çözüm potansiyeli sunmaktadır. Özellikle Türkiye'deki Kızıldere gibi volkanik kökenli jeotermal sahalar, doğal olarak yüksek CO_2 içeriğine sahiptir. Normalde atmosfere salınan bu gaz, çevresel açıdan zararlı bir emisyon kaynağıdır. Bunun yerine, sistemde toplanarak yeniden kuyuya enjekte edilmesi hem sera gazı emisyonlarını azaltmakta hem de üretim kapasitesini artırmakta kullanılabilir.

CO_2'nin termo-fiziksel özellikleri, onu jeotermal gaz kaldırma için son derece uygun kılmaktadır. Yüksek basınçlarda su içerisinde çözünürlüğü oldukça fazladır. Kuyu tabanında çözünmüş halde bulunan CO_2, akışkan yüzeye doğru yükselirken basıncın düşmesiyle birlikte çözünürlüğünü kaybeder ve çözeltiden ayrılarak kabarcıklar oluşturmaya başlar. Bu kabarcıklar sıvı yoğunluğunu düşürerek kolonun kaldırılmasına katkıda bulunur. Bu sürece, basınç-sıcaklık-çözünürlük etkileşimiyle belirlenen "flash noktası" adı verilir. Kuyu içerisindeki CO_2 miktarının kontrol

edilmesiyle, bu noktanın derinliği ve yoğunluk azalmasının büyüklüğü ayarlanarak kuyu başı basıncı ve üretim debisi optimize edilebilir.

Bu çalışmada öncelikle, Duan ve Sun (2003) tarafından geliştirilen termodinamik model kullanılarak CO_2 çözünürlüğü hesaplanmıştır. Bu model; fugasite, iyonik etkileşimler ve kimyasal potansiyel değişimlerini dikkate almakta ve jeotermal koşullarda yüksek doğruluk sağlamaktadır. Hesaplamalar için Python tabanlı bir yazılım geliştirilmiş ve 2000 bar basınca, 533.15 K sıcaklığa kadar geniş bir aralıkta test edilmiştir. Çözünürlük modeli iki aşamada doğrulanmıştır:

1. Duan ve Sun'un yayınladığı teorik sonuçlarla kıyaslanarak tutarlılık sağlanmıştır.
2. Wiebe ve Gaddy (1935, 1940) tarafından gerçekleştirilen deneysel verilerle karşılaştırılarak gerçek koşullar altında doğruluğu test edilmiştir.

Doğrulanan çözünürlük modeli daha sonra bir kuyu basınç profili simülasyon aracına entegre edilmiştir. Bu modelde, yerçekimi ve sürtünme kaynaklı basınç kayıpları, CO_2 kütle fraksiyonunun yoğunluk üzerindeki etkisi ve sıcaklık gradyanları dikkate alınmıştır. Veri girişleri; kuyu geometrisi, ölçülmüş kuyu tabanı basınç-sıcaklık değerleri, CO_2 konsantrasyonları ve akışkan özelliklerinden oluşmuştur.

Model Türkiye'deki farklı jeotermal sahalardan üç kuyuya uygulanmıştır:

- AF-21 (Afyon, 300 m) → sığ rezervuar örneği
- OB-16 (Germencik, 1200 m) → orta derinlikte rezervuar
- K-49 (Kızıldere, 3165 m) → derin ve yüksek sıcaklıklı rezervuar

Tüm kuyularda, simülasyon sonuçları ile saha ölçümleri arasında yüksek uyum elde edilmiştir. Özellikle K-49 kuyusunda %3 çözünmüş CO_2 oranında, model ile ölçülen basınç profilleri büyük ölçüde örtüşmüştür.

Duyarlılık analizleri, CO_2 kütle fraksiyonu arttıkça flash noktasının daha derinlere kaydığını göstermiştir. Ayrıca farklı CO_2 oranları ve debilerinin kuyu başı basıncına etkisi incelenmiş; CO_2 oranının artışıyla basıncın doğrusal biçimde yükseldiği, ancak sabit bir oranda debi artırıldığında başlangıç basıncının düştüğü ve artış eğiminin azaldığı belirlenmiştir. Ayrıca belirli bir konsantrasyonun ötesinde ek CO_2 enjeksiyonunun marjinal fayda sağlamadığı tespit edilmiştir. Bu sonuç, gaz kaldırma sistemlerinin tasarımında optimum CO_2 enjeksiyon oranlarının belirlenmesinin kritik olduğunu ortaya koymaktadır.

Çalışmanın çevresel boyutu da dikkate değerdir. Günümüzde birçok jeotermal santral, buhar ayrıştırmasından sonra açığa çıkan NCG'leri (çoğunlukla CO_2) atmosfere salmaktadır. Bu çalışmada önerilen yöntemle, açığa çıkan CO_2'nin geri kazanılıp kuyuya enjekte edilmesi hem sera gazı emisyonlarını azaltmakta hem de santral üretimini artırmaktadır. Böylece çevresel sürdürülebilirlik ile ekonomik verimlilik aynı sistem içinde bütünleşmektedir. Ayrıca, mekanik pompa ihtiyacının ortadan kalkması veya azalması; yatırım maliyetlerini, bakım sürelerini ve arıza risklerini düşürerek özellikle yüksek sıcaklıklı rezervuarlarda işletme güvenilirliğini artıracaktır.

Sonuç olarak, bu çalışma CO_2 gaz kaldırma yönteminin, özellikle yüksek sıcaklık ve yüksek NCG içeren jeotermal sahalarda uygulanabilir ve sürdürülebilir bir yapay kaldırma tekniği olduğunu göstermektedir. Geliştirilen çözünürlük modeli ile kuyu basınç simülasyonlarının entegrasyonu, sistem performansını öngörmede güvenilir bir araç sunmaktadır. Sonuçlar, kontrollü CO_2 enjeksiyonunun kuyu başı basıncını

yükseltebileceğini, akışkan debilerini artırabileceğini ve kuyuların üretim ömrünü uzatabileceğini ortaya koymaktadır. Gelecekte saha ölçekli pilot uygulamalar ile sistem tasarımı, uzun dönem performans doğrulaması ve ekonomik fizibilite analizleri yapılmalıdır. Bu tür çalışmalar, CO_2 gaz kaldırma yöntemini yenilikçi bir yapay kaldırma tekniği olarak jeotermal endüstride konumlandırabilir.

1. INTRODUCTION

Geothermal wells especially the ones found in volcanic regions like Kizildere in Turkey often produce fluid with high content of non-condensable gases (NCGs), mostly being composed of carbon dioxide (Canbaz et al., 2022). This influences the wellbore pressure, phase behavior, and chemical interactions (Sevindik, 2023). A critical aspect of geothermal well performance lies in the behavior of fluids within the reservoir and wellbore, particularly when these fluids contain dissolved gases, such as carbon dioxide. The flow dynamics of geothermal water with carbon dioxide has been a subject of growing interest because of their implications for production efficiency. (Ma et al., 2017) studied the CO_2 dissolution process under high pressure showing time dependence in solubility. This thesis explores the effect of CO_2 on the flow performance of geothermal wells, with the aim of enhancing production while leveraging the unique properties of this gas.

Studies have shown that CO_2 solubility generally increases with pressure and decreases with temperature, though the temperature effect is more complex (Spycher et al., 2003); (Pistone et al., 2011). For instance, Duan and Sun ((2003) observed that at lower temperatures, solubility increases as temperature drops, while at higher temperatures and pressures, solubility may increase with temperature due to pressure's dominance. Over time, different models have been developed to estimate CO_2 solubility under varying temperatures and pressures, including those by (Duan et al., 2006), (Mao et al., 2013), and (Zhaoa et al., 2015), each with varying levels of accuracy.

The flow of fluids in Geothermal wells resembles the flow of fluids in petroleum wells. So, when the geothermal fluid moves up the well as it does in oil and gas wells, momentum and heat loss occur and as a result pressure drop is experienced and we have less wellhead pressure at the surface. The pressure loss often leads to flashing and formation of two-phase regions along the well (Hasan and Kabir, 2010). Study by García et al (2002) during the flow of CO_2 rich geothermal fluids, from the bottom to the surface, its static pressure decreases, and the following processes occurs. The CO_2 content in the fluid exceeds the solubility of CO_2 under the new pressure; hence, CO_2

is released from the solution to form gaseous bubbles. When this process occurs, single phase flow transitions to double-phase flow, and since the static pressure continues decreasing, more CO_2 is released.

Two-phase flow is a simultaneous movement of two distinct phases, typically a liquid and a gas within the same flow channel, where the phases interact across a shared interface. The most common form in industrial applications is the liquid-gas system, characterized by a deformable interface where mass and heat transfer occur and can vary significantly. These interfacial configurations are known as flow regimes (Mohammed, 2014). In geothermal wells, fluid flow typically transitions through key flow regimes, bubbly, slug, churn, and annular-like of those found in oil and gas systems (Hasan and Kabir, 2010). Research on geothermal fluids shows that dissolved CO_2 plays a significant role in two-phase flow behavior. Early studies in fields like East Mesa (California) revealed that dissolved CO_2 affects the onset of gas breakout, where gas separates from the liquid within the wellbore. Pistone et al., (2011) stressed that phase changes caused by solubility can affect flow dynamics and pressure gradients in geothermal systems with dissolved CO_2. Their results correspond with extensive multiphase transport models, such as those developed by Vafai et al., (2007), which offers a theoretical framework for interfacial mass and energy transfer in complex geothermal settings.

In more recent years there have been increasing investigations CO_2 enhanced geothermal systems (CO_2-EGS) which focuses on CO_2 as a working fluid, highlighting its favourable thermophysical properties, such as low viscosity and high expansibility, which enhance flow velocities and reduce pumping energy demands required to circulate CO_2 leading to potentially high heat extraction efficiencies (Shi et al., 2019). Studies have also emphasized CO_2's role in reducing mineral precipitation compared to water-based systems, offering the dual benefit of improved operational efficiency and reservoir sustainability. Despite these advancements and studies on CO_2 as a working fluid, the application of CO_2, specifically in geothermal gas lift systems, remains underexplored. Gas lift, a well-established artificial lift technique in the oil and gas industry, involves injecting gas in the annulus between tubing and casing where it will enter the tubing through a gas-lift valve located in a side pocket to reduce the hydrostatic pressure of the fluid column by reducing the density of the reservoir fluid, thereby enhancing the fluid flow from the bottom of the wellbore to the surface

(Egu D I et al., 2023) . In geothermal contexts, the decline of naturally occurring non-condensable gases (NCGs), including CO_2, often leads to reduced performance over time, particularly in high-temperature reservoirs, where pumps may be impractical owing to thermal and mechanical constraints. This brings the need for an artificial lift technique to aid the flow of fluids to the surface. Although nitrogen (N_2) in form of air or liquid has been employed as a gas lift medium in some geothermal fields (Andersen et al., 1988), such as The Dieng Geothermal Field, in Indonesia (Kamila et al., 2024), the use of CO_2, an abundant and naturally present gas in many geothermal systems, presents an opportunity for a more integrated and sustainable approach. The interplay between CO_2 solubility, phase behaviour, and flow characteristics in geothermal water underscores the need for understanding of its potential as a gas lift agent. A recent study by (Aydin & Merey, 2024) presented findings on gas lifting in geothermal wells using Alaşehir field in western Turkey, as a case study. Their work demonstrated that gas lift could be used as a feasible alternative artificial lift method to electrical submersible pumps (ESPs) and line shaft pumps (LSPs) which are often limited in high temperature and deviated wells. Utilizing PIPESIM software for performance modeling, the authors conducted extensive sensitivity analyses examining the effects of various design parameters such as gas type (CO_2 vs. N_2), injection depth, gas injection rate, tubing diameter, and valve configurations on production performance.

2. LITERATURE REVIEW ON GEOTHERMAL WELLBORE MODELLING

Different models have been developed to predict the pressure and temperature traverse in geothermal wellbores. Cinar et al (2006) developed a multi-feed P-T wellbore model for geothermal wells and accounted for change in density and wellhead pressure due to change in CO_2 mass fractions. This model has been instrumental in formulating our model, especially for the single-phase region.

However, geothermal wellbores typically exhibit two-phase flow behavior, particularly after the onset of flashing. Predicting pressure drop in these conditions has long relied on empirical and mechanistic models. Among the foundational studies, Orkiszewski's (1967) correlation remains a cornerstone in two-phase vertical flow modeling, accounting for varying flow regimes and their associated pressure gradients through experimentally derived correlations. Originally designed for petroleum uses, it has been adopted for geothermal wells as well.

Geothermal wells however have non-condensable gases, high temperature and high enthalpy making them exhibit different flow behaviors as compared to petroleum systems. Recognizing this, Hasan and Kabir (2010) developed a drift-flux-based modeling framework, offering a more generalized treatment of two-phase flow that accounts for mass and heat transfer simultaneously. Their model captures the key phenomena of pressure drop, heat loss to the formation, and steam flashing processes which are especially relevant in high-temperature wells.

Further refinement of drift-flux modeling was pursued by Acuña and Arcedera (2005), who compared homogeneous and drift-flux models for interpreting Pressure-Temperature-Spinner (PTS) survey data in geothermal wells. They found that at high velocities, simplifications in the frictional loss and holdup terms could still yield sufficiently accurate mass and enthalpy distributions. Notably, their field applications demonstrated the capability of these models to resolve feed zone contributions, a critical factor in geothermal well performance analysis.

Recent work by Lei et al. (2023) specifically applied a drift flux approach to simulate two-phase flow in the Yangbajing geothermal field. Their study emphasized the necessity of incorporating slip velocity between gas and liquid phases. Homogeneous models, which neglect this slip, resulted in considerable deviations from measured wellhead pressures and temperatures. By comparing three variations of the drift flux model, they demonstrated how model choice impacts the predicted flash depth and hence calcite scaling tendencies, highlighting the importance of model selection in scaling-prone fields.

Beyond drift-flux and empirical models, simulation-based tools such as HOLA, T_2 Well, and WELLSIM have gained traction. These tools integrate field data with numerical solvers to model pressure and temperature gradients under various production and reinjection scenarios. They have been used effectively to match measured P-T profiles and to assess feed zone behaviors, even under complex CO_2-rich or scaling conditions ((Vasini et al., 2018);(Lei et al., 2023)).

Awad and Muzychka (2008) proposed several new definitions for two-phase viscosity in homogeneous flow models, drawing analogies from effective thermal conductivity in porous media and viscosity in two phase flow. These definitions ensure that the viscosity transitions correctly between liquid and vapor limits as mass quality changes, addressing a common shortcoming in earlier models. Their approach was validated against extensive experimental data of flow in circular pipes, mini channels, and microchannels. Among the models tested, the Effective Medium Theory and Maxwell-Eucken 2 definitions yielded the lowest error margins, offering improved accuracy in predicting frictional pressure drops. Their work enhances the applicability of homogeneous models in geothermal wellbore simulations, particularly where computational simplicity is needed.

In addition to the previous models, advancements have introduced more comprehensive numerical models aimed at minimizing the discrepancies observed in earlier predictive methods. One notable contribution in this regard is the work by Ojo and Fadairo (2024), who developed a new model for predicting pressure traverse in two-phase flow geothermal wells by incorporating all significant pressure drop components due to accumulations, frictions, static heads, and accelerations within the wellbore.

This inclusion of pressure drop due to accumulation marks a key advancement, as many traditional models including those by Orkiszewski (1967), Ansari et al. (1994), and even Hasan and Kabir (2010) either ignore or oversimplify this term. The proposed model by Ojo and Fadairo (2024) builds upon the energy conservation framework and extends it with a more physically realistic representation of transient behaviors, capturing pressure surges at the onset of production and flow regime transitions, which older models often fail to address.

Their model was validated against field data from two well-known geothermal wells (KE1-22 and Mesa 6-1), where it achieved remarkably low mean absolute relative errors of 0.033 and 0.052, respectively. In contrast, the Hasan-Kabir model showed errors around 0.12–0.17, while Orkiszewski's and Homogeneous models yielded even larger deviations. This strong agreement between modeled and measured pressure profiles underscores the accuracy of the proposed model, especially under complex two-phase and transient flow conditions.

While early empirical models provide a practical starting point, modern drift-flux and numerical approaches offer enhanced precision, especially under high enthalpy and multiphase conditions. Continued refining of these predictive tools remains essential.

3. STATEMENT OF THE PROBLEM

Declining pressure generally limits the operation of geothermal wells, which over time causes inadequate natural lift and decreased fluid flow to the surface. Because of their high temperatures, corrosive fluids, and inclination, traditional artificial lift techniques such as downhole pumps face major difficulties in geothermal wells, which makes them expensive and unreliable. Although CO_2 is a common component of geothermal fluids and has been investigated as a working fluid in EGS (Esteves et al., 2019), its use as a gas lift medium to boost production in geothermal wells lacks enough study. The problem lies in the limited understanding of how the CO_2 impacts the wellhead pressure, two-phase flow dynamics and flash point changes.

Moreover, existing models and calculation methods often assume the validity of Henry's law, which becomes increasingly inaccurate under the elevated temperature and pressure conditions typical of geothermal wells. To address this limitation, our model incorporates Duan's equation, which provides more accurate predictions at high pressures and temperatures, particularly for determining the flash point pressure.

Also, despite the advancement in developing empirical wellbore models, a gap remains in integrating these models into custom-coded simulators. Most existing studies rely on commercial tools (e.g., UniSim, PIPESIM, and OLGA OLGA, TOUGH2, PROSPER) or black-box software e.g WELLFLO, which may limit transparency and computational experimentation. This thesis seeks to bridge the existing knowledge gap by developing and validating an in-house coded model to simulate wellbore pressure profiles in geothermal wells producing CO_2-rich brines. Furthermore, the thesis evaluates the feasibility and efficacy of using CO_2-based gas lift systems as a novel method to sustain and enhance geothermal energy production, offering an integrated approach that combines flow modelling with energy optimization strategies.

4. METHODOLOGY

This study aims to develop a computational model to establish a link between wellhead pressure and bottomhole pressure in geothermal wells containing water with dissolved CO_2. Central to this relationship is the solubility of CO_2 in water as a function of temperature and pressure.

4.1 Duan's CO_2 Solubility Model

To accurately model CO_2 solubility in geothermal water, the thermodynamic model proposed by Duan and Sun (2003) was adopted. This model is widely recognized for its reliability in predicting CO_2 solubility in water under a wide range of geothermal conditions.

A Python-based numerical tool was developed to compute CO_2 solubility at temperatures up to 533.15 K and pressures up to 2000 bar. The results from the code developed were validated in two steps:

- Theoretical validation: The computed solubility values were cross verified against the data reported in Duan and Sun (2003).
- Experimental validation: Additional comparison was made with the historical experimental results from Wiebe and Gaddy (1935; 1940), which cover a similar range of temperature and pressure.

The solubility behavior of CO_2 in water with temperature at various pressure levels is illustrated in Figure 2.

The CO_2 solubility calculation follows the Duan's solubility equation:

$$ln m_{CO_2} = ln y_{CO_2} \varphi_{CO_2} P - \mu^{I(0)}{}_{CO_2}/RT - 2\,\lambda_{CO_2-Na}(m_{Na}+m_K+2m_{Ca}+2m_{Mg}) - \zeta_{CO_2-Na-Cl}\, m_{Cl}(\, m_{Na} + m_K + m_{Ca} + m_{Mg}\,) + 0.07 m_{SO_4} \quad (4.1)$$

Where:

- m_{CO_2} is the molality of dissolved CO_2

- y_{CO_2} is the CO_2 mole fraction in the gas phase
- φ_{CO_2} is the fugacity coefficient of CO_2 in the gas phase
- P is the pressure
- $\mu^{I(0)}{}_{CO_2}$ is the standard chemical potential
- R is the universal gas constant, and T is the absolute temperature
- λ, ζ, and other parameters represent interaction coefficients and ionic molalities of Na^+, K^+, Ca^{2+}, Mg^{2+}, Cl^-, and SO_4^{2-}

4.2 Well Pressure Profile Model

To simulate the pressure profile along a geothermal wellbore, a numerical model was developed that accounts for:

- Gravitational pressure loss
- Frictional pressure loss

The model is structured as a stepwise iterative algorithm, calculating pressure gradients from bottomhole to wellhead for different CO_2 mass fractions.

Model Inputs:

- Well geometry
- Bottomhole pressure and temperature
- CO_2 concentration
- Fluid physical properties (e.g., density, viscosity)
- Thermal properties for temperature profile calculation

4.3 Implementation

The model was coded in Visual Studio Code and executed using Python. It computes pressure distributions along the well and generates a pressure profile. These computed results are then visually compared with digitized field data on the same plot for direct validation.

5. DUAN MODEL

5.1 Description of the Model

The Duan's CO_2 solubility model, developed by Duan and Sun in 2003, is a thermodynamic model that can precisely predict the amount of carbon dioxide gas that can dissolve in geothermal water at a given temperatures and pressures over a wide range of pressures and temperatures. This model is reliable and widely used for simulating CO_2 solubility in geothermal fluids.

The Duan's equation, described in the previous chapter, considers fugacity, pressure, temperature, and the ionic strength of the water solution. This study's model can predict CO_2 solubility in pure water by assuming no interactions between dissolved salts and CO_2.

5.2 Model Against Model Validation of The CO2 Solubility Code

To check the validity of the CO_2 solubility code Duan's 2003 results over a wide range of pressures and temperatures represented in Figure 5.1 below were compared with the code calculated results and the comparison was plotted in Figure 5.2 below.

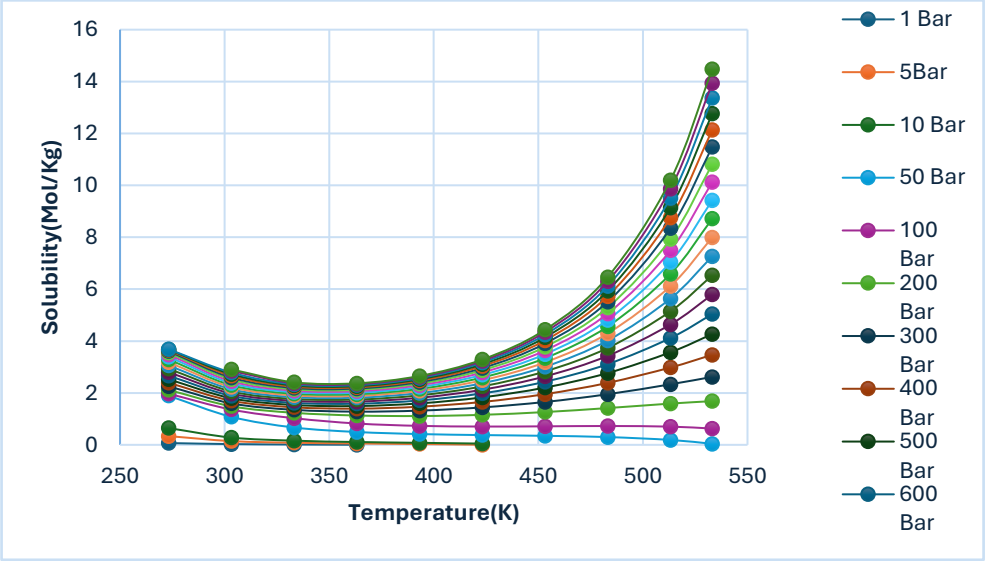

Figure 5.1 : Modeling Solubility data of CO_2 in water under various temperature and pressure conditions by Duan (2003).

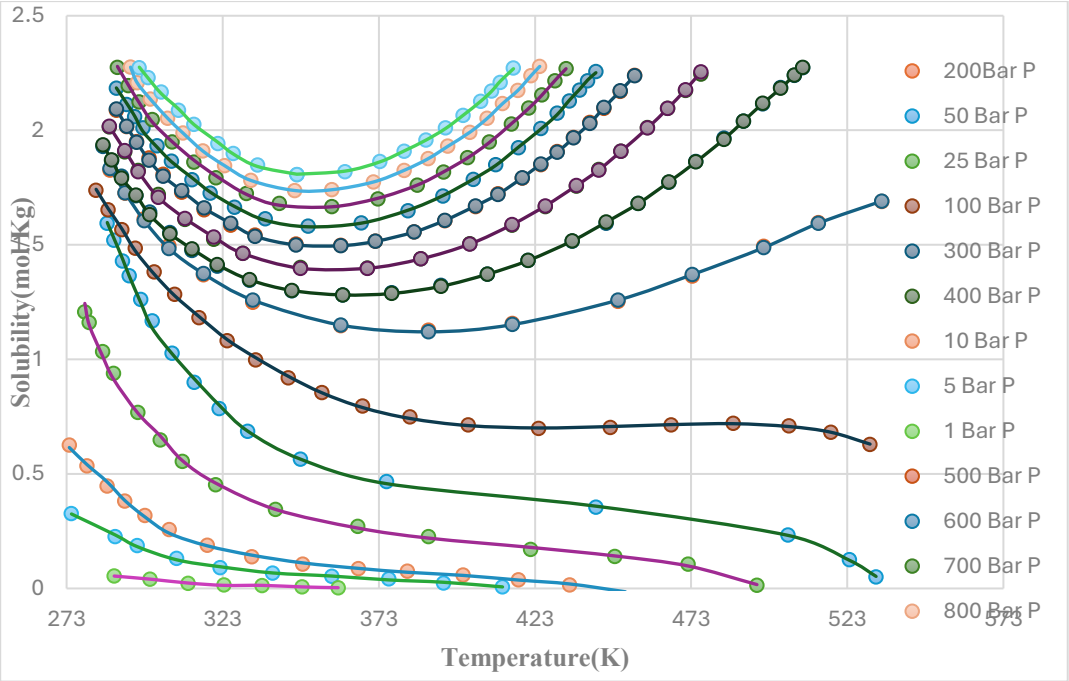

Figure 5.2 : Comparison between Duan's CO_2 solubility data and code calculated CO_2 solubility in water from 273.15K to 533.15K and pressures up to 900bar.

Figure 5.2 above represents the comparison between Duan's CO_2 solubility data and code calculated CO_2 solubility in water from 273.15K to 533.15K and pressures up to 900bar.The plotted results indicate how the model accurately predicts CO_2 solubility behaviour over a wide range of temperatures and pressures. The code successfully replicates Duan's isobaric solubilities of CO_2 in pure water graph.

5.3 Model Against Experimental Data Validation of the CO2 Solubility Code

The figure 5.3 A and B below represent the comparison between the experimental results, Duan's model, and the findings of this study at 40^0C (A) and 50^0C (B), highlighting the reliability of our results. From the figures, the CO_2 solubility in this study shows a better match compared with results from (Ji et al., 2024) at 40^0C and 50^0C. Furthermore, the code calculated results in this study align well with calculated solubility using Duan's model.

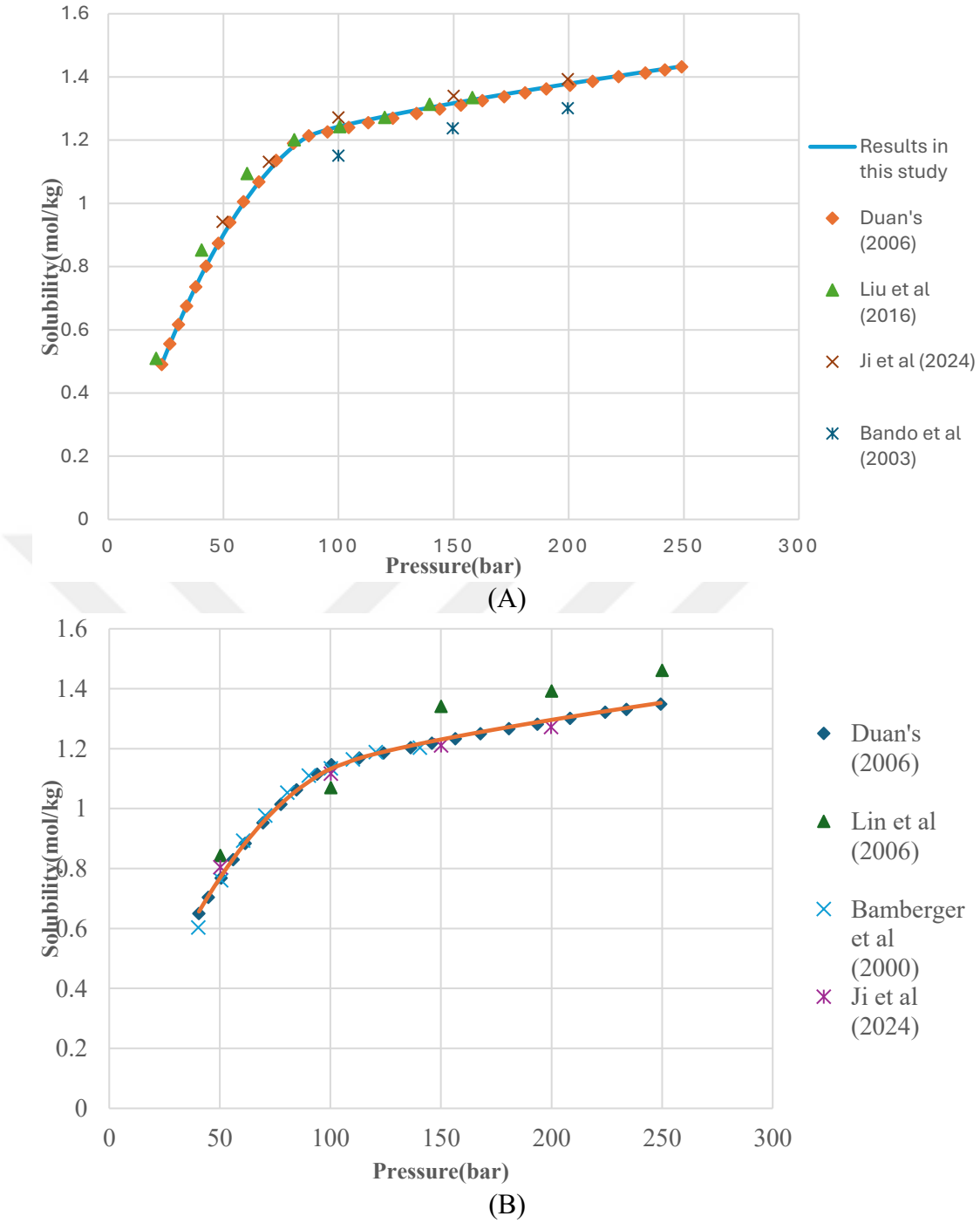

Figure 5.3 : A comparison of CO_2 solubility between the code calculated values in this study and those published in the literature at 40^0C (A) and 50^0C (B) respectively. The solid lines represent the solubility values calculated by using Duan's model.

6. FLASH POINT PRESSURE AND CO_2 MASS FRACTIONS RELATIONSHIP

Dissolved CO_2 gas has effect on density as well as pressure. Figure 6.1 below was plotted using Duan's model and shows the effect of varying CO_2 mass fraction on flash point pressure. As the mass fraction of CO_2 increases the flashpoint pressure shifts deeper into the reservoir. In the pressure profile, what this means is that as we increase the amount of CO_2 the flash point will go further deeper in the pressure profile, leading to a shift in the pressure profile above the flash point in the two-phase region. This will move the wellhead pressure to the right and the flash point depth deeper.

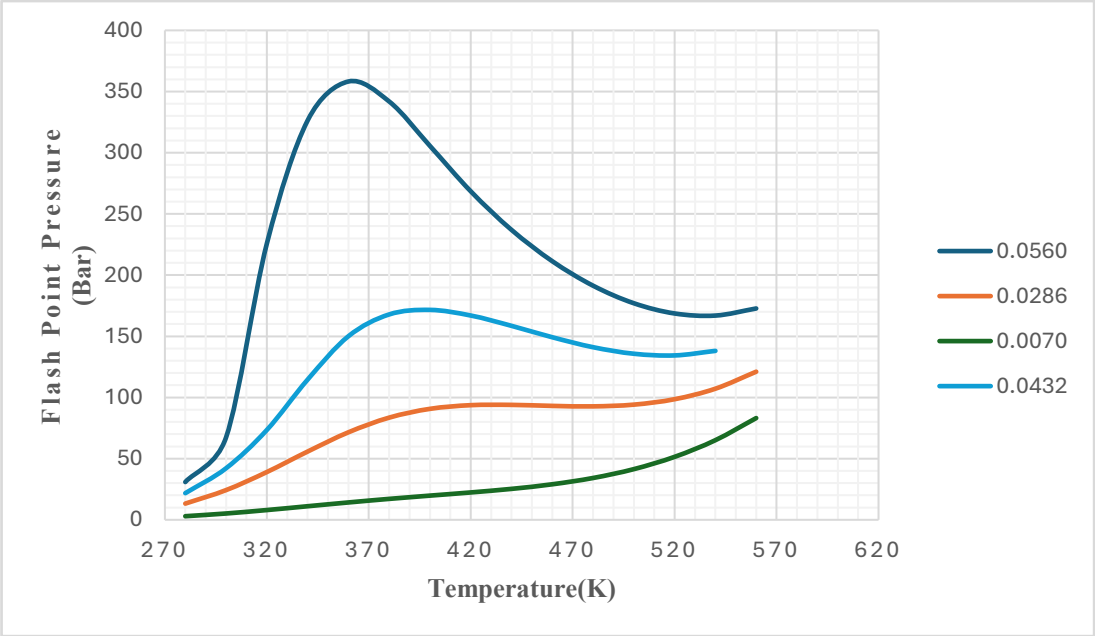

Figure 6.1 : Effect of changing mass fractions to flash point pressure.

7. WELL PRESSURE PROFILE MODEL

During production, a typical pressure profile is given in Figure 5. The lower sections of the well show single-phase region, which means that only liquid water exists. The pressure profile follows a straight line and steeper trend because of the hydrostatic gradient.

At a certain depth, flashing occurs, and a two-phase region begins. The flashing point represents the pressure and depth at which the flow of liquid water changes from a single-phase flow phase to a double phase flow.

In geothermal wells which produce fluids with dissolved CO_2, the gas phase in the two-phase region is consists of both steam and CO_2.

The flashing point occurs in the region where the deviation from the straight line begins. This is where the pressure profile slope becomes less steep. In the double phase region, the slope of the pressure profile changes a lot because the gas phase is less dense than the liquid phase. This difference in density changes the hydrostatic pressure gradient, which makes the pressure profile gradient less steep as you go higher up the well.

In the double region, the gas bubbles' expansion increases the gas-liquid mixture volume and decreases the overall density. As a result, the pressure does not drop as quickly as it does in the single-phase region, which gives the pressure profile a curved curvature.

Figure 7.1 below serves as a visualization model, to help with visualization of the necessary parameters.

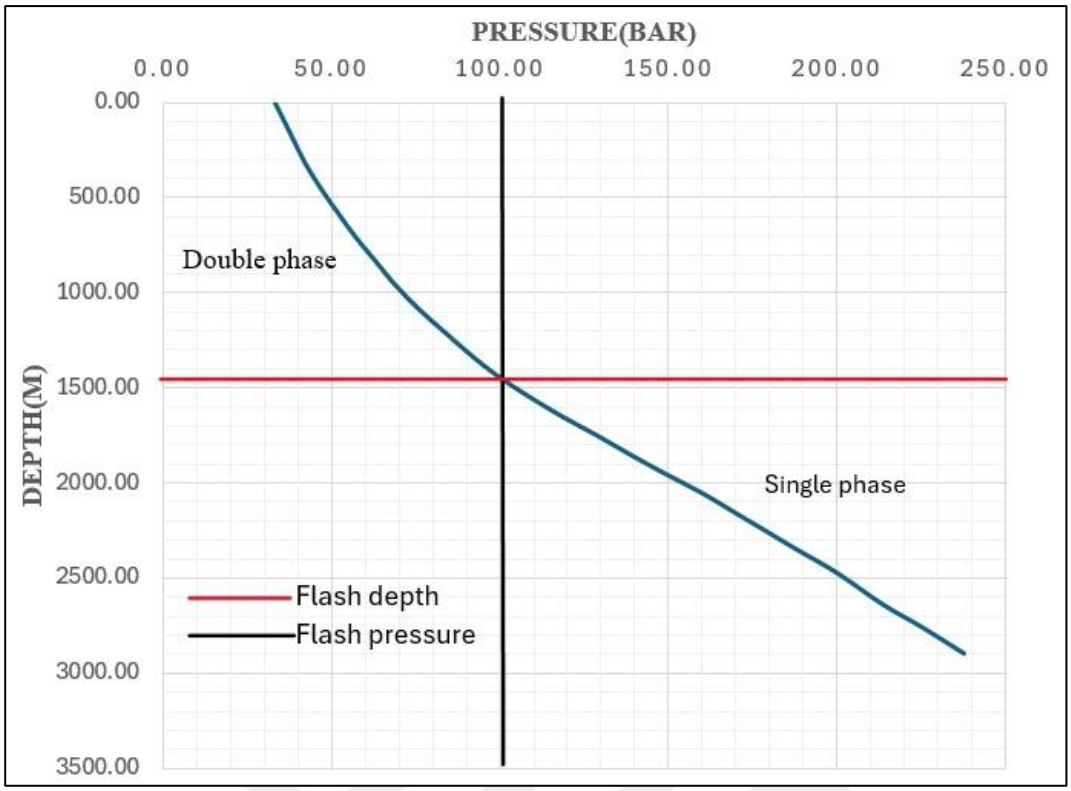

Figure 7.1 : Pressure-depth profile illustrating flash point depth and pressure in a geothermal well.

The figure above shows the transition from single-phase liquid flow to a double-phase flow (liquid + steam/CO_2) as pressure decreases with depth. The flash point depth (red line) and flash point pressure (black line) mark the onset of this phase change.

7.1 Numerical Model Execution

A python code has been developed in the visual code studio platform to model the flow behavior of the geothermal fluids in vertical wells. The model developed in this study can generate the pressure profile for wells that produce water with dissolved CO_2.

The existing and known, well parameters, including well depth, fluid properties and bottom hole pressure and temperature conditions, are used as input parameters for the developed pressure profile code. The numerical model gets executed in the visual code studio platform, simulating the expected pressure behavior along the wellbore under the given conditions. The computed pressure profile is then plotted on the same graph as the digitized field data for a direct visual comparison.

7.2 Validation of the Well Model

To ensure the reliability and accuracy of the developed geothermal well pressure profile code, a validation process was carried out using real field data from three geothermal wells: AF-21 from Afyon by Cinar et al (2006), OB-16 from Germencik by Tureyen et al (2014) and K-49. These wells were chosen due to the availability of well-documented pressure profiles, making them ideal for testing the performance of the numerical model.

In this section, the validity of the model will be tested by comparing the data of the AF-21, OB-16 and K-49 wells with the model data using this program. Then, the model will be applied for various situations and how the pressure and temperature change with other variables will be examined.

7.2.1 Validation of the model to the AF-21 well

The AF-21 well is found in the Afyon region, Ömer-Gecek field in Turkey. The well was drilled in 1997 and has been producing intermittently since then. It produces a water-gas (CO_2) mixture fluid at the wellhead. The well is 212 m deep.

Table 7.1 : The input parameters of the A-21 well.

***kh*, md-ft**	500
***re*, ft**	1000
***PR*, psia**	2000
T_{bh}, °F	250
S	0
P_{wf} , psia	500
***t*, day**	30
***L*, ft**	1000
α, ft²/day	0.96
k_e , Btu/ft-day- °F	33.60
Geothermal gradient, °F/ft	0.18
c_w, Btu/lbm- °F	1
θ^o	90
r_w, ft	0.40

7.2.2 Data acquisition and digitization

Since the original well pressure profiles were presented in graphical form in published studies, a digitization process was done to the pressure profile of the well by

plotdigitizer platform. The digitized AF-21 well data was then plotted and compared to the code model results. Figure 7.2 gives the results of the comparison of the model developed in this study to the AF-21 well. As it is clear, the model developed in this study provides a good match to the actual field data. Figure 7.1 gives the results of the pressure profile after changing the CO_2 gas mass fraction. The result in this figure shows that as the CO_2 mass fraction is increased the flash point depth moves deeper down into the well.

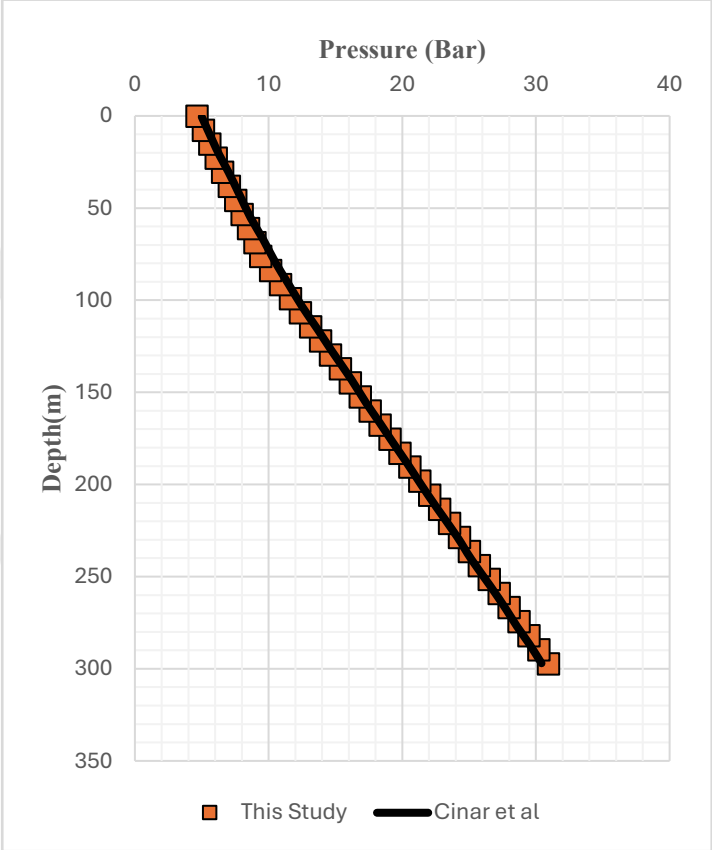

Figure 7.2 : The pressure profile of the AF-21 well and the model, where the mass fraction of the dissolve CO_2 is at 0.9%.

7.3 Validation of the Model to the OB-16 Well

The Germencik geothermal field is situated in the western region of the Buyuk Menderes Graben in Western Anatolia. The field was identified by MTA (General Directorate of Mineral Research and Exploration) in 1968 and since that time more than 38 wells have been drilled. The reservoir is predominantly liquid, with temperatures nearing 240 °C, characterized by a significant noncondensable gas concentration, primarily CO_2. OB-16 well is one of the wells at Germencik field, it has about 3.21% dissolved CO_2 and the flashing happens at about 666m.

7.3.1 Data acquisition and digitization

A digitization approach was applied to OB-16 well pressure profile available in the published study by Tureyen et al (2014) numerical data points for comparison were extracted. The pressure-depth profile of the OB-16 well was then plotted in Excel as indicated in figure 7.3, preserving the accuracy of the field-measured values. The code model calculated pressure-depth profile of the OB-16 was plotted on the same graph for matching, and the results are as shown in the Figure below. Again, a good match is obtained at 3.21% dissolved CO_2.

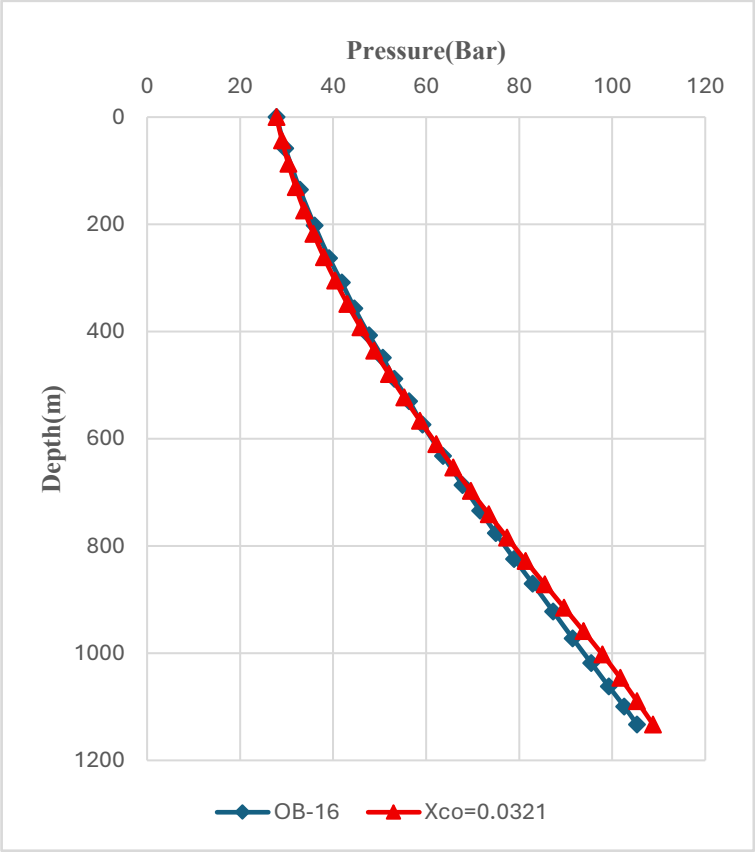

Figure 7.3 : The pressure profile of the OB-16 well and the model, where the mass fraction of the dissolved CO_2 is at 3.21%.

7.4 Validation of the Model to the K-49 Well

KD-49 is one of the wells found in the Kizildere Geothermal Field in Turkey. It is a 3178.5 m deep, 8 ½ inch well and has about 260 bottom hole flowing pressure, 241 ^{0}C bottom hole temperature and 1.3662 ft³/s Flow rate.

Using the model in this study the field data from the K-49 well was analysed to look for a good match between the calculated and measured data. By varying the CO_2 mass

fraction, a fairly good match was found at 3% CO_2 mass fraction. Also, the flashing point was found to be approximately 1061 m. The results are presented in Figures 7.4 below.

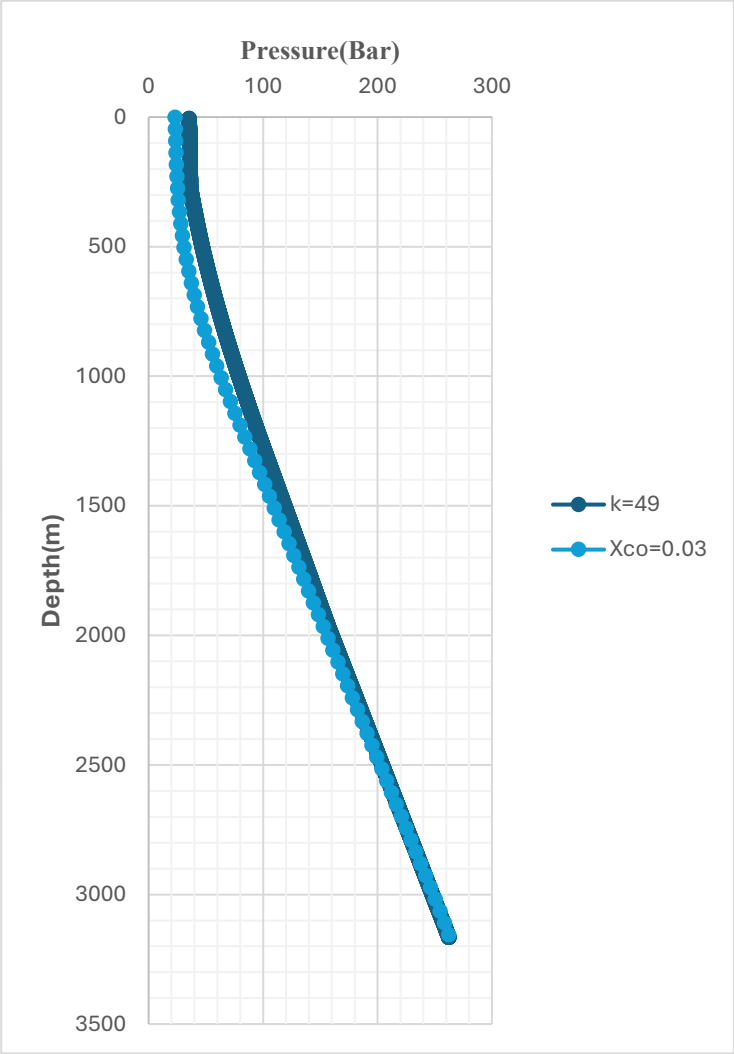

Figure 7.4 : Comparison between code model computed and K-49 measured pressure profile.

8. DETAILS OF THE MODEL USED IN THIS STUDY

8.1 Description of the Code

A flow chart of the code is given in Figure 8.1 outlines the key computational stages, including input initialization, function definitions, single-phase and two-phase flow simulations, and finalizing the computation. A brief description of the steps involved in the coding process is included below:

1. Divide the total well depth into several intervals.
2. Assume a pressure drop for the interval.
3. Calculate fluid properties using average pressure.
4. Calculate the pressure drop using single phase liquid.
5. Compared with assumed pressure drop, if the difference is less than 0.001 proceed to the next step (convergence), otherwise repeat from step 4 (divergence).
6. Once the pressure match has been obtained proceed with the next interval.
7. Check if the calculated pressure is still less than the Duan's flash point pressure otherwise transition to double-phase flow correlations.
8. The calculations end when the total wellhead is reached.

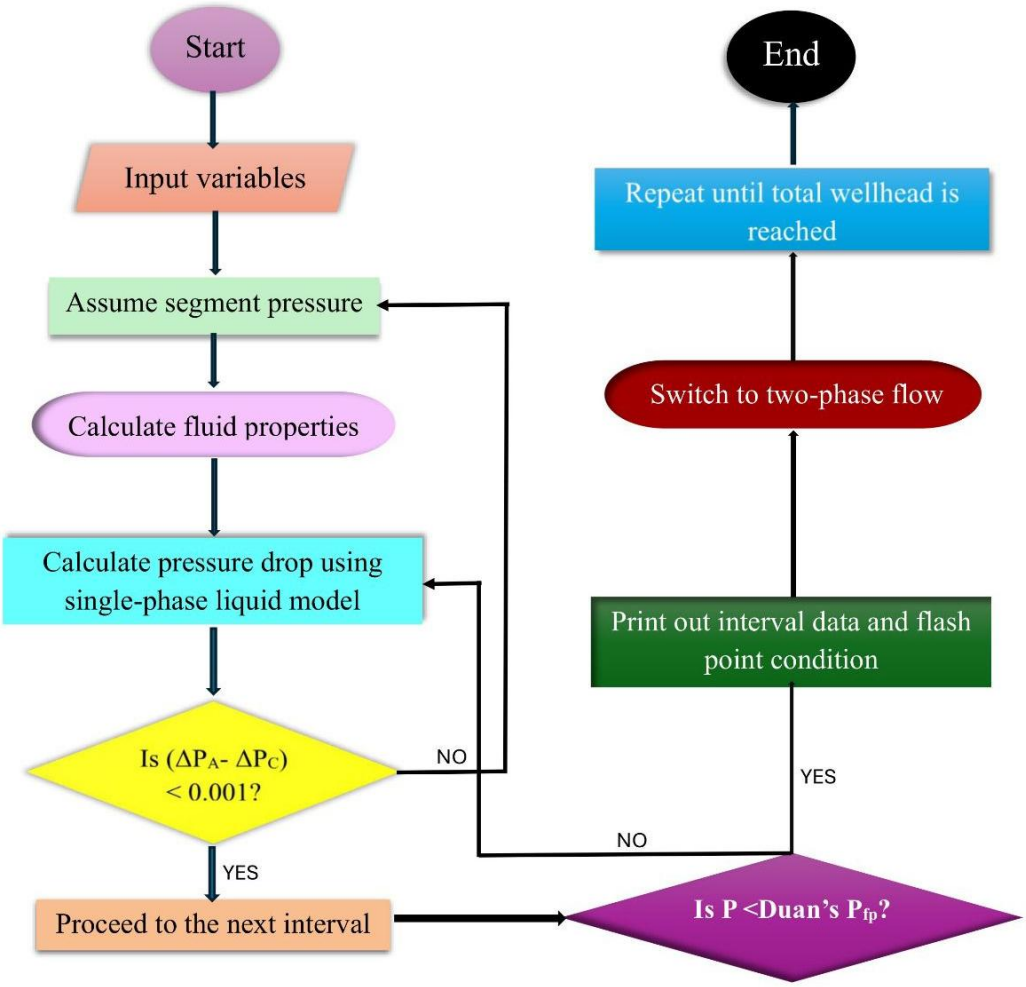

Figure 8.1 : Flowchart for computing the wellbore pressure profile.

8.2 Equations of Pressure and Temperature Used for The Code

8.2.1 Single phase flow

The calculation of heat transfer during injection of a single-phase liquid or gas into a well was presented by Ramey (1962 and 1964). Although analyses were derived for liquid and gas individually, in practical terms the difference between them is so small that the analysis for liquid flow may be used for both liquid and gas (Horne, n.d.)

Ramey's equation describing the temperature behaviour as the fluid move up the wellbore is given by the following equation,

$$T=(T_{ei}- az) + (T_i- T_{ei})* e^{-z/A^!} + a A^! (1-e^{-z/A^!}) \quad (8.1)$$

where z is the distance upwards from the bottom of the well, T_o is the inflowing fluid temperature, Tei is the downhole reservoir temperature (usually equal to T_i) and a is

the geothermal gradient (the increase of formation temperature with increase in depth). $A^{!}$ is a "Diffusion depth," and is a slowly varying function of time, t, given by:

$$A^{!}(t)=) \frac{wcf(t)}{2\pi k} \tag{8.2}$$

f(t) is dimensionless time function and is given by the following equation,

$$Log[f(t)]= 0.007165+ 0.30947*Log(t_D)- 0.04807*[Log(t_D)]^2+0.003574*[Log(t_D)]^3 \quad \text{for } 10^{-2} \leq t_D \leq 10^4 \tag{8.3}$$

Where,

$$t_D = \frac{\alpha t}{(r_2')^2} \tag{8.4}$$

We will adopt the following equations from (Cinar et al., 2006) to calculate the pressure drops, Temperature, water density and Viscosity segment wise.

The pressure drop for single-phase flow can be calculated using the following equation,

$$P_{wf}\text{-P}= \rho g L + \frac{8}{\pi^2}\frac{f\rho q^2}{d^5}\text{L} \quad \text{T(K)}, \rho(\frac{kg}{m^3}) \tag{8.5}$$

Where,

- f is the average friction factor (calculated using Reynolds number)
- ρ is the average fluid density
- g is the gravity acceleration
- d is the pipe diameter
- q is the flow rate

Friction single phase,

$$f_{=} \frac{1.325}{\left[ln\left(\frac{e}{3.7D}+5.74N_{Re}^{-0.9}\right)\right]^2}, \text{ e=0.00008} \tag{8.6}$$

$$N_{Re}=\frac{\rho v D}{\mu}$$

The liquid density (lb/ft^3) is calculated using the following equation dependent on Temperature

For temperature T≤ 410K

$$\rho_{L=0.06272796}\frac{1000}{1.16849-0.001477T+3.0564410^{-6}T^2}\ \text{T(K)} \tag{8.7}$$

Else,

$$\alpha = 1.29463 * (1-\frac{T}{647.35})^{0.28571}\quad \text{T(K)} \tag{8.8}$$

$$\rho_{L=}357.0 * 0.06242796 * e^{\alpha} \tag{8.9}$$

The liquid viscosity is calculated using the following equation also dependent on Temperature.

$$\mu=\frac{2.185}{0.04012T+5.154710^{-6}T^2}\quad \mu(cp), T(F) \tag{8.10}$$

8.2.2 The study on the flash point pressure in a wellbore

Duan's model and New Raphson method were used to determine the flash point pressure

8.2.3 Double phase flow

For the section above the flash point the pressure loss for the double-phase flow is given by the equation below.

$$P_o\text{-P}=\rho_m g dz+\frac{8}{\pi^2}\frac{f_m\rho_m q^2}{d^5}\text{dz}\quad \text{T(K)}, \rho(\frac{kg}{m^3}) \tag{8.11}$$

Where,

- f_m=0.025, Friction factor for the mixture, in our case assumed to be constant,
- P_o represents the initial pressure, for the double phase flow it represents the flash point pressure, so P_o=P_{fp}
- P_{fp} is the flash point pressure
- dz represents segment length
- ρ_m represents mixture density
- ρ_m Two-phase mixture density
- $\rho_m = f_L\rho_L$+(1-f_L) ρ_g
- $\rho_L$is the density of the liquid phase
- $\rho_g$is the density of the gas phase

- f_L is Liquid holdup
- f_L=$1 - f_g$
- ρ_g=ρ_c
- ρ_c=is the CO_2 gas density
- CO_2 density in (lb/ft^3) is given by the following equation,

$$\rho_{CO2}=\frac{0.06242796*1}{\left(\frac{188.82*T.k}{P\_pascal)}\right)+\left(\frac{0.0824+0.00000001249*P\_pascal)}{(0.01*T.K)^{\frac{10}{3}}}\right)}\text{P (pascal)} \quad (8.12)$$

- $f_g$is the gas hold up, a fraction occupied by gas

$$f_g = \left[\left(\frac{v_{sg}}{C_O*v_m+v_{tr}}\right]\right. \quad (8.13)$$

- v_{sg} stands for gas phase superficial velocity
- v_m stands for mixture velocity given by v_m= q_t/A
- v_{tr} stands for terminal velocity and given by the following Equation

$$v_{tr} = 1.53* \left[\left(\frac{g(\rho_L-\rho_g)\sigma}{{\rho_L}^2}\right]\right.^{0.25} \quad (8.14)$$

Gravity(g)= 32, C_o=1.2, Surface Tension (σ)= 0.0696

Double Phase Temperature Equation,

$$T=(T_{ei}- aL)+ (T_i- T_{ei})e^{(-L/A!)}+ aA^!(1-e^{(-L/A!)})-g/c * A^! (1-e^{(-L/A!)}) \quad (8.15)$$

9. RESULTS AND DISCUSSION

The comparison between the field-measured pressure profiles and the numerically simulated results revealed a good agreement between the three datasets:

- For the AF-21 well (300m depth, Afyon field), the simulated pressure profile closely followed the trend of the measured data, demonstrating the model's ability to replicate real-world well behavior in relatively shallow geothermal systems.
- Similarly, for the OB-16 well (1200m depth, Germencik field), the predicted pressure profile aligned well with the digitized field data, confirming that the model remains valid even for deeper geothermal wells with more complex pressure dynamics.
- For the K-49 (3165m depth), a good match was achieved at 3%. The model pressure profile followed closely the pressure profile data of K-49 well, again highlighting how the model remains valid in deep geothermal wells.

The good match observed between the simulated and actual well-pressure profiles validates the accuracy of the developed code. The minor discrepancies observed can be attributed to uncertainties in field measurements, variations in geothermal reservoir properties, or assumptions made in the modeling process.

9.1 Sensitivity Analysis

In this chapter, we conduct a comprehensive sensitivity analysis to explore the influence of varying carbon dioxide mass fractions on the flash point pressure and the depth at which this flash point occurs within the wellbore. The analysis focuses on modelling pressure profiles for two wells, each subjected to different CO_2 concentrations and flow rate, to better understand the thermodynamic and flow implications of CO_2-rich geothermal fluids. Analysis of the influence of varying flow rates on the well-head pressure has also been conducted.

9.1.1 Influence of varying co₂ mass fractions on flash point pressure and depth

As would be predicted in a real wellbore, raising the amount of dissolved CO_2 causes the flash point to move to deeper depths. As a result, a higher pressure would be needed to keep the CO_2 dissolved. Because of this, the pressure profile above the flash point shifts toward higher pressures. Consequently, at a given depth, the pressure at each point in the well above the flash point rises compared to when there is less CO_2.

Figure 9.1 and 9.2 below show the pressure-depth profiles for two wells at different CO_2 levels. Figure 9.3 shows as expected how the flash point depth increases deeper as the mass fraction is increased. Each figure shows how the flash point location has changed and how that has affected pressure gradients.

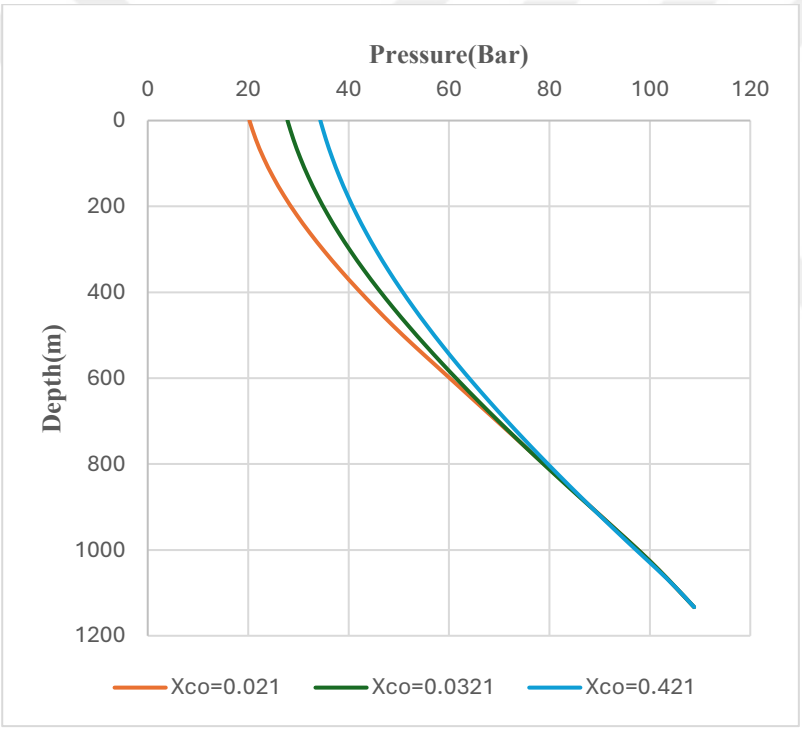

Figure 9.1 : Results of the pressure profile of the OB-16 well with various CO_2 mass fractions.

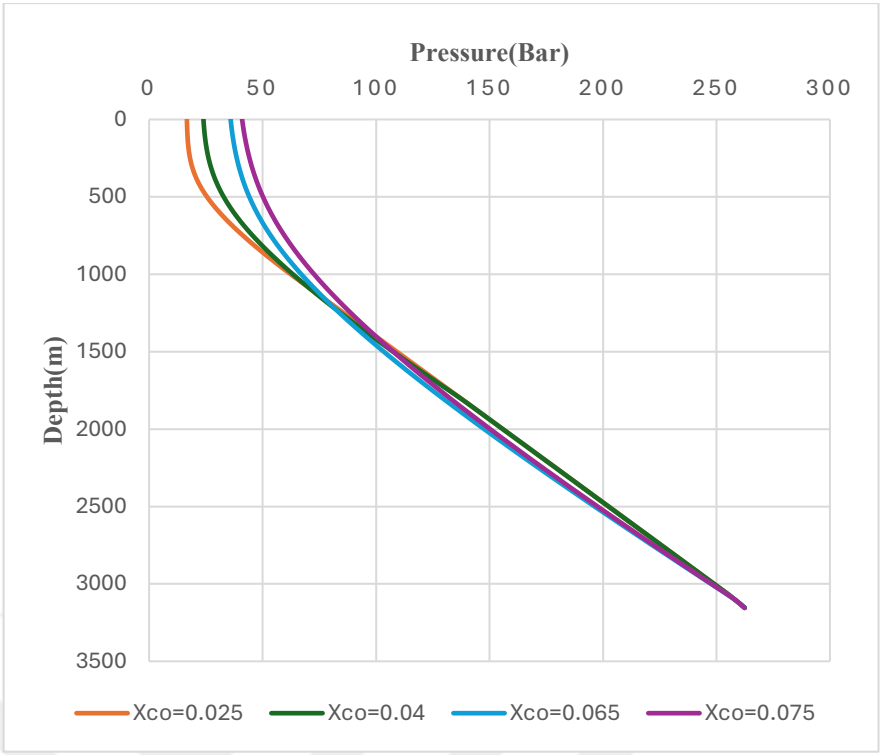

Figure 9.2 : Results of the pressure profile of the K-49 well with various CO_2 mass fractions.

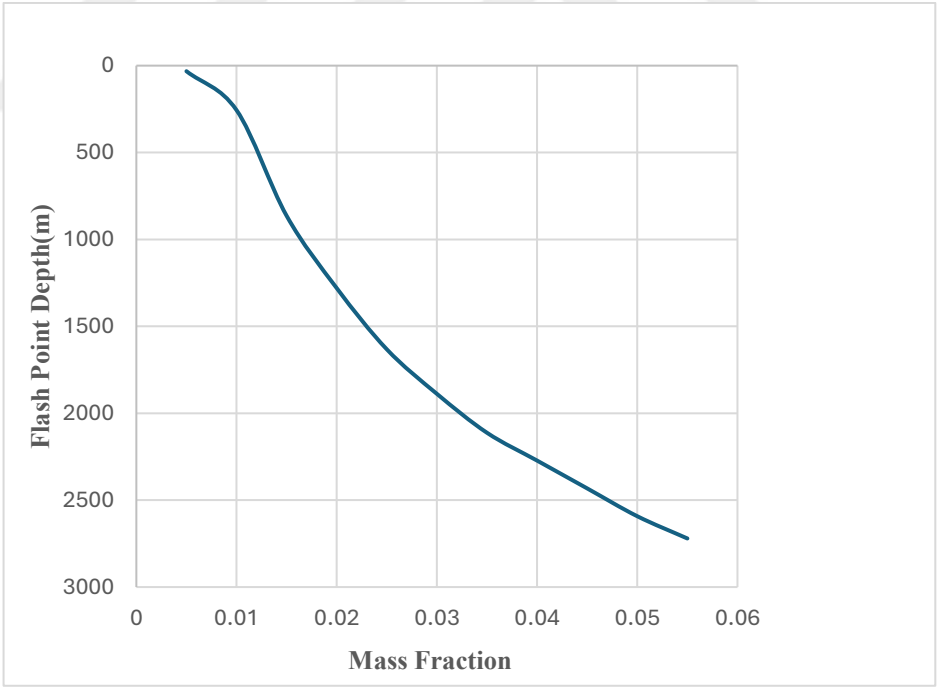

Figure 9.3 : Results of flash point depth with various CO_2 mass fractions.

9.1.2 Influence of varying co₂ mass fractions and flow rates on wellhead pressure

The wellhead pressure increases linearly with the mass fraction of CO_2 at all flow rates. This means that a higher amount of CO_2 in the geothermal fluid raises the pressure at

the wellhead. This is because CO_2 changes the density and the phase behavior of the fluid. But as the flow rate increases less pressure is achieved at the well-head.

In Figure 9.4 below the wellhead pressure starts lower at about 10 Bar at lower flow rates and rises steeply as the mass fraction increases, reaching about 45 Bar at 0.06 mass fraction. When the flow rates is increased from 5 kg/s to 50 kg/s at a given mass fraction, the initial wellhead pressure goes down, and the pressure-rise with mass fraction becomes less steep. This shows that higher flow rates lead to lower well-head pressure.

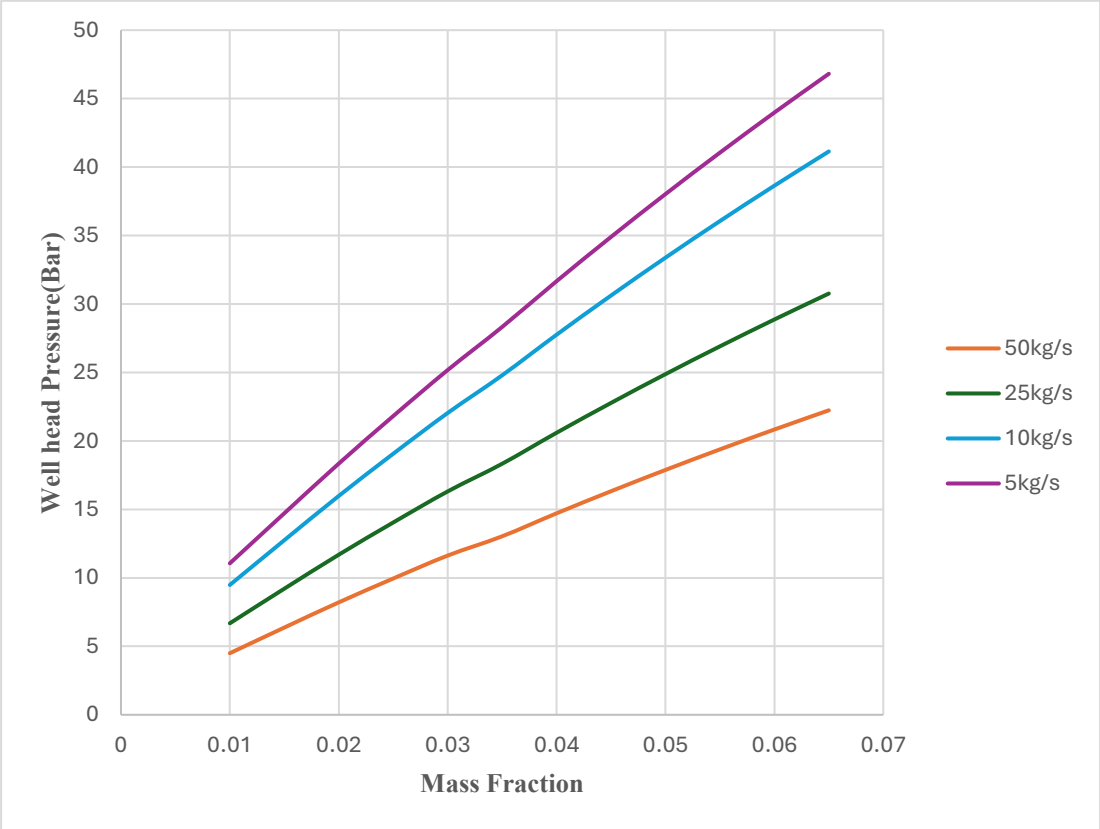

Figure 9.4 : Results of wellhead pressure with various CO_2 mass fractions and flow rates.

10. INFLUENCE OF VARYING CO_2 MASS FRACTIONS ON GEOTHERMAL FLUID DENSITY

The influence of varying dissolved CO_2 mass fractions to the density in geothermal fluids was investigated by changing the initial CO_2 mass fraction and analyzing at the resulting density profiles. Three mass fractions were considered in this case 0.02, 0.0221, and 0.026, as illustrated in Figure 10.1 below. In the deeper part of the wellbore, where the system stays in a single-phase state, the density of the fluid doesn't vary much when the CO_2 mass fraction changes. The profile in this phase don't change much, which means that dissolved CO_2 doesn't have a significant effect on the fluid density at higher pressures during the single-phase flow.

However, as the fluid rises and enters the two-phase zone, there is a clear change in density profile. At the onset of flashing the pressure decreases below the saturation level, which causes the dissolved CO_2 to be released. This change in phase causes the density of the fluid to drop sharply and exponentially. It's worth noting that a larger CO_2 mass fraction causes a bigger decline in density, as seen by the Xco = 0.026 curve being more different from the rest. This pattern is in line with what would be expected: gas evolution lowers the total density since there is a less dense vapor phase.

Overall, the results show how important CO_2 exsolution is for geothermal fluid dynamics. They also show that even small increases in the initial CO_2 level can have a significant effect on the density profile and mobility of fluids in the two-phase region.

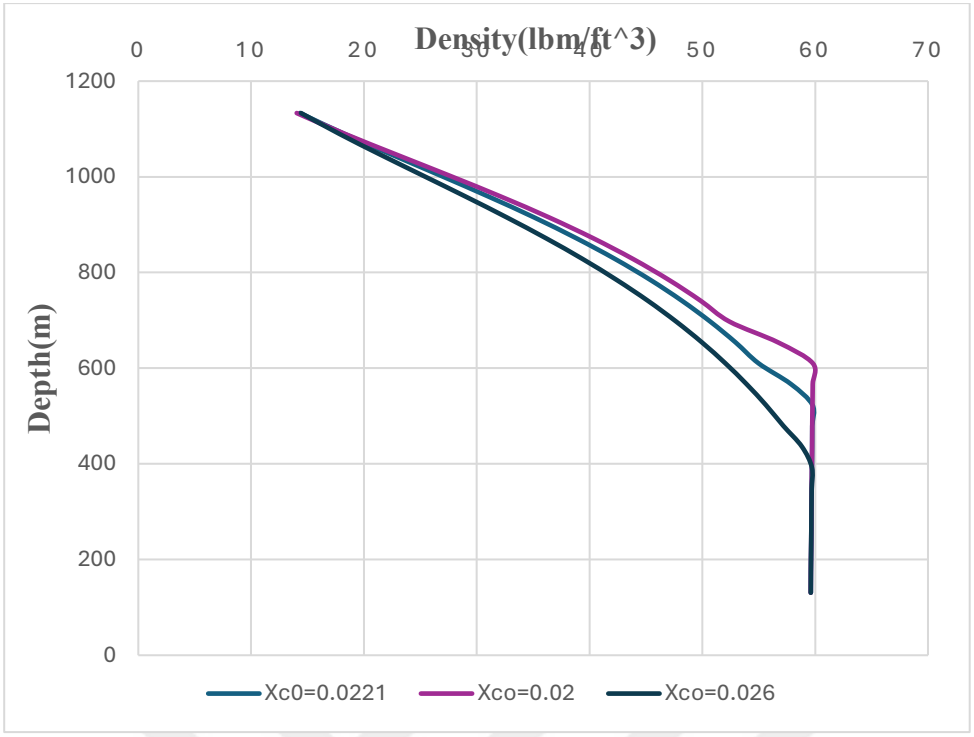

Figure 10.1 : Results of Influence of varying CO_2 mass fractions on Fluid Density.

11. CONCLUSION

A CO_2 solubility code was developed based on Duan's 2003 equation of state. The results obtained from the model demonstrated high accuracy when compared with experimental and modeling data, maintaining an error margin within 0.04% in the temperature range of 273 to 533 K and pressures up to 2000 bar. The model effectively predicts CO_2 solubility in water under geothermal conditions, making it a reliable tool for designing CO_2-based gas lift systems. The model can also be used to predict the flash point pressure and CO_2 mass fraction retained in liquid phase during the double phase flow in geothermal wells.

Furthermore, a geothermal well pressure profile code was designed to simulate the pressure behavior of geothermal wells under different CO_2 mass fractions. This numerical model accounted for pressure losses due to friction, gravity, and kinetic energy effects along the wellbore. The simulation results indicated that increasing CO_2 mass fractions effectively reduced pressure losses and contributed to higher wellhead pressures, thereby enhancing well productivity. The stepwise computational approach incorporated thermodynamic property calculations, phase transition modeling, and iterative pressure drop calculations to accurately represent real-world well conditions.

The findings of this study suggest that CO_2 gas lift systems could serve as an efficient and cost-effective alternative to conventional artificial lift methods in geothermal wells. By improving flow rates and increasing energy production efficiency, the integration of CO_2 gas lift can lead to significant operational advantages, including lower maintenance costs and reduced energy consumption.

In conclusion, this research successfully validates the potential of CO_2 gas lift systems for geothermal wells through both theoretical modeling and numerical simulations. The developed solubility model and well pressure profile code offer valuable computational tools for optimizing gas lift design in geothermal energy production. Future work should focus on experimental validation, field-scale implementation, and further exploration of CO_2 phase behavior under varying geothermal conditions. By advancing the understanding and application of CO_2 gas lift, this study paves the way

for the adoption of innovative and sustainable solutions in geothermal energy production.

REFERENCES

Acuña, J. A., & Arcedera, B. A. (2005). Two-phase flow behavior and spinner data analysis in geothermal wells. In *Thirtieth Workshop on Geothermal Reservoir Engineering*.

Andersen, G. R., Pye, S. D., Probst, A. A., & of Calif Assignee, all. (1988). Gas lift process for restoring flow in depleted geothermal reservors.

Ansari, A. M., Sarica, C., Shoham, O., & Brill, J. P. (1994). A Comprehensive Mechanistic Model for Upward Two-Phase Flow in Wellbores.

Awad, M. M., & Muzychka, Y. S. (2008). Effective property models for homogeneous two-phase flows. *Experimental Thermal and Fluid Science*, *33*(1), 106–113.https://doi.org/10.1016/j.expthermflusci.2008.07.006

Aydin, H., & Merey, Ş. (2024). Gas lifting design and application in geothermal wells: A case study from West Anatolia, Turkiye. *Geoenergy Science and Engineering*, *233*. https://doi.org/10.1016/j.geoen.2023.212544

Canbaz, C. H., Ekren, O., & Aksoy, N. (2022). Review of wellbore flow modelling in CO_2-bearing geothermal reservoirs. In *Geothermics* (Vol. 98). Elsevier Ltd. https://doi.org/10.1016/j.geothermics.2021.102284

Cinar, M., Onur, M., & Satman, A. (2006). development of a multi-feed p-t wellbore model for geothermal wells. In *Proceedings, Thirty-First Workshop on Geothermal Reservoir Engineering*.

Duan, Z., & Sun, R. (2003). *An improved model calculating CO_2 solubility in pure water and aqueous NaCl solutions from 273 to 533 K and from 0 to 2000 bar*. www.elsevier.com/locate/chemgeo

Duan, Z., Sun, R., Zhu, C., & Chou, I. M. (2006). An improved model for the calculation of CO_2 solubility in aqueous solutions containing Na^+, K^+, Ca^{2+}, Mg^{2+}, Cl^-, and $SO4^{2-}$. *Marine Chemistry*, *98*(2–4), 131–139. https://doi.org/10.1016/j.marchem.2005.09.001

Egu D I, Ilozobhie A J, Obalola, H. A., & Okpata, J. B. (2023). Gas Lift Modeling: A Viable Option for Oil Production Optimization. In *Asian Journal of Applied Science and Technology (AJAST)* (Vol. 7, Issue 4).

García, A., Espinosa-Paredes, G., & Barragán, R. Ma. (2002). Effect of non-condensable gases on the flow of water and steam in geothermal wells. *Geofísica Internacional*, *41*(4), 377–383. http://www.redalyc.org/articulo.oa?id=56841404

Hasan, A. R., & Kabir, C. S. (2010). Modeling two-phase fluid and heat flows in geothermal wells. *Journal of Petroleum Science and Engineering*, *71*(1–2), 77–86. https://doi.org/10.1016/j.petrol.2010.01.008

Horne, R. N. (1988). *Geothermal Energy Assessment*.

Ji, Z., Wang, H., Wang, M., Lv, W., Wang, S., Kou, Z., He, C., & Wang, L. (2024). Experimental and modeling study of CO_2 solubility in formation brines at in-situ conditions. *Journal of Cleaner Production*, *438*. https://doi.org/10.1016/j.jclepro.2024.140840

Kamila, Z., Elfajrie, I., Supijo, M., Herdian, R., Dwiyatmoko, N., Istiawan Nurpratama, M., & Ashat, A. (2024). Aldevco Octagon 2nd Floor. In *PT Geo Dipa Energi (Persero)* (Issue 75).

Lei, H., Xie, Y., Li, J., & Hou, X. (2023). Modeling of two-phase flow of high temperature geothermal production wells in the Yangbajing geothermal field, Tibet. *Frontiers in Earth Science*, *11*. https://doi.org/10.3389/feart.2023.1019328

Ma, X., Abe, Y., Kaneko, A., Fujimoto, S., & Murakami, C. (2017). Study on dissolution process of liquid CO_2 into water under high pressure condition for CCS. *Energy Procedia*, *114*, 5430–5437. https://doi.org/10.1016/j.egypro.2017.03.1687

Mao, S., Zhang, D., Li, Y., & Liu, N. (2013). An improved model for calculating CO_2 solubility in aqueous NaCl solutions and the application to CO_2-H_2O-NaCl fluid inclusions. *Chemical Geology*, *347*, 43–58. https://doi.org/10.1016/j.chemgeo.2013.03.010

Mohammed, I. Y. (2014). modeling and simulation of multiphase system in production well using WellFlo R software. In *Research Article International Journal of Current Engineering and Technology* (Vol. 4, Issue 6). http://inpressco.com/category/ijcet

Ojo, I., & Fadairo, A. (2024). A new model for predicting pressure traverse in two phase flow geothermal well. *Geoenergy Science and Engineering*, *240*. https://doi.org/10.1016/j.geoen.2024.213029

Orkiszewski, J. (1967). *Predicting two-phase pressure drops in vertical pipe*. https://doi.org/https://doi.org/10.2118/1546-PA

Pistone, S., Stacey, R., & Horne, R. (2011). The significance of CO_2 solubility in geothermal reservoirs. In *Proceedings, Thirty-Sixth Workshop on Geothermal Reservoir Engineering*.

Sevindik, D. B. (2023). Predictive reservoir modeling for CO_2 sequestration in kizildere reservoir using multiple inter-well tracer tests a thesis submitted to the graduate school of natural and applied sciences of middle east technical university.

Shi, Y., Song, X., Wang, G., McLennan, J., Forbes, B., Li, X., & Li, J. (2019). Study on wellbore fluid flow and heat transfer of a multilateral-well CO_2 enhanced geothermal system. *Applied Energy*, *249*, 14–27. https://doi.org/10.1016/j.apenergy.2019.04.117

Spycher, N., Pruess, K., & Ennis-King, J. (2003). CO_2-H_2O mixtures in the geological sequestration of CO_2. I. Assessment and calculation of mutual solubilities from 12 to 100°C and up to 600 bar. *Geochimica et Cosmochimica Acta*, *67*(16), 3015–3031. https://doi.org/10.1016/S0016-7037(03)00273-4

Tureyen, O. I., Sarak, H., Gulgor, A., Satman, A., Tureyen, O. I., and Erkan, B. (2014). *A study on the production and reservoir performance of the germencik geothermal field*. https://www.researchgate.net/publication/267895332

Vafai, K., Faghri, A., & Zhang, Y. (2007). Transport phenomena in multiphase systems. *international journal of heat and mass transfer*, *50*(13–14), 2857–2858. https://doi.org/10.1016/j.ijheatmasstransfer.2006.12.008

Vasini, E. M., Battistelli, A., Berry, P., Bonduà, S., Bortolotti, V., Cormio, C., & Pan, L. (2018). Interpretation of production tests in geothermal wells with T2Well-EWASG. *Geothermics*, *73*, 158–167. https://doi.org/10.1016/j.geothermics.2017.06.005

Zhaoa, H., Fedkin, M. V., Dilmore, R. M., & Lvov, S. N. (2015). Carbon dioxide solubility in aqueous solutions of sodium chloride at geological conditions: Experimental results at 323.15, 373.15, and 423.15K and 150bar and modeling up to 573.15K and 2000bar. *Geochimica et Cosmochimica Acta*, *149*, 165–189. https://doi.org/10.1016/j.gca.2014.11.004

APPENDIX

APPENDIX A: Pressure profile code

APPENDIX A: Pressure profile code

```
# Helper Functions

import math
import numpy as np

def liquid_density(T_K):
    if T_K <= 410.0:
        denom = (1.16849 - 0.001477 * T_K + T_K ** 2 * 3.05644e-6)
        return 0.06242796 * 1000.0 / denom
    else:
        alf = 1.29463 * ((1.0 - T_K / 647.35) ** 0.28571)
        return 357.0 * 0.06242796 * math.exp(alf)

def viscosity(T):
    return 2.185 / ((0.04012 * T) - 1 + 0.0000051547 * T**2)

def pressure_drop(P_prev, d_av, d_L, f, q_t, r):
    return P_prev - (d_L * d_av / 144.0) - (0.0001748 * d_L * f * d_av * q_t**2 / (2.0 *
rw)**5)

def reynolds(w, rw, v_w):
    return 0.263136 * w / (v_w * rw)

def friction_factor(NR):
    return 1.325 / (math.log(0.000030604 + 5.74 * NR**-0.9)**2.0)

def dimensionless_time(alpha, t, r2):
    return (alpha * t) / (r2 ** 2)

def f_t(td):
    log_td = math.log10(td)
    log_ft = (0.007165 + 0.30947 * log_td - 0.04807 * log_td**2 + 0.003574 * log_td**3)
    return 10 ** log_ft

def diffusion_depth(w, c, ft, ke):
```

```
    return (w * c * ft) / (2 * math.pi * ke)

def temperature_profile_single_phase(Tei, Ti, a_geo, z, A_prime):
    return ((Tei - a_geo * z) + (Ti - Tei) * math.exp(-z / A_prime) + (1 - math.exp(-z /
A_prime)) * a_geo * A_prime)

def temperature_profile_double_phase(Tei, Ti, a_geo, L, A_prime, g, c):
    return ((Tei - a_geo * L) + (Ti - Tei) * math.exp(-L / A_prime) + a_geo * A_prime * (1 -
math.exp(-L / A_prime)) - (g / c) * A_prime * (1 - math.exp(-L / A_prime)))

def terminal_velocity(rho_L, rho_G):
    g = 32.152
    sigma = 0.0696
    return 1.53 * (((g * (rho_L - rho_G) * sigma) / (rho_L ** 2)) ** 0.25)

def holdup(v_sg, vm, rho_L, rho_G):
    vtr = terminal_velocity(rho_L, rho_G)
    C = 1.2
    return 1.0 - (v_sg / (C * vm + vtr))

def antoine_water_pressure(T_celsius):
    pressure_mmHg = 10 ** (8.07131 - 1730.63 / (T_celsius + 233.426))
    return 0.0001333224 * pressure_mmHg  # MPa

def henry_constant(T_celsius):
    return math.exp(
        4.517428673 +
        2.554534e-2 * T_celsius -
        1.02213e-4 * T_celsius ** 2 +
        9.30689e-8 * T_celsius ** 3
    )

def calculate_XCO2(P_psi, T_celsius):
    P_mpa = P_psi * 0.006894757
    Ps = antoine_water_pressure(T_celsius)
    K = henry_constant(T_celsius)
    P_CO2 = P_mpa - Ps
```

```
    return P_CO2 * (44.0 / (K * 18.0))

def calculate_PH2O(T):
    Tc, Pc = 647.29, 220.85
    c1, c2, c3, c4, c5 = -38.640844, 5.8948420, 59.876516, 26.654627, 10.637097
    t = (T - Tc) / Tc
    return (Pc * T / Tc) * (1 + c1*(-t)**1.9 + c2*t + c3*t**2 + c4*t**3 + c5*t**4)

def velocity_sg(q_t, rho_L_bh, X, Xco, rw, P, T):
    rho_CO2 = density_co2(P, T)
    return (q_t * rho_L_bh * X * (1.0 - Xco)) / (math.pi * rw ** 2 * rho_CO2)

def density_co2(P, T_C):
    T_K = T_C + 273.15
    P_bar = P * 0.0689476
    co2_density_functions = {
        373.15: lambda P: 0.0401 * P - 0.0047,
        473.15: lambda P: 0.0317 * P - 0.0146,
        573.15: lambda P: 0.0261 * P + 0.0025,
        673.15: lambda P: 0.0222 * P - 0.0116
    }

    available_temperatures = sorted(co2_density_functions.keys())

    if T_K in co2_density_functions:
        return co2_density_functions[T_K](P_bar)

    if T_K < available_temperatures[0]:
        return co2_density_functions[available_temperatures[0]](P_bar)

    if T_K > available_temperatures[-1]:
        return co2_density_functions[available_temperatures[-1]](P_bar)

    T1 = max([T for T in available_temperatures if T < T_K])
    T2 = min([T for T in available_temperatures if T > T_K])

    rho1 = co2_density_functions[T1](P_bar)
```

```
    rho2 = co2_density_functions[T2](P_bar)
    return rho1 + (rho2 - rho1) * ((T_K - T1) / (T2 - T1))

# Duan & Zhang coefficients
a = np.array([
    8.99288497e-2, -4.94783127e-1, 4.77922245e-2, 1.03808883e-2, -2.82516861e-2,
    9.49887563e-2, 5.20600880e-4, -2.93540971e-4, -1.77265112e-3, -2.51101973e-5,
    8.93353441e-5, 7.88998563e-5, -1.66727022e-2, 1.398, 2.96e-2
])

r = 8.314467  # Universal gas constant (J/mol/K)
pc = 73.8     # Critical pressure (bar)
tc = 304.2    # Critical temperature (K)

def fun(tr, vr, pr):
    tr2, tr3 = tr**2, tr**3
    vr2, vr4, vr5 = vr**2, vr**4, vr**5
    term1 = (a[0] + a[1]/tr2 + a[2]/tr3) / vr
    term2 = (a[3] + a[4]/tr2 + a[5]/tr3) / vr2
    term3 = (a[6] + a[7]/tr2 + a[8]/tr3) / vr4
    term4 = (a[9] + a[10]/tr2 + a[11]/tr3) / vr5
    term51 = a[12] / (tr3 * vr2)
    term52 = a[13] + a[14] / vr2
    term53 = np.exp(-a[14] / vr2)
    term5 = term51 * term52 * term53
    return pr * vr / tr - 1 - term1 - term2 - term3 - term4 - term5

def duanz(pr, tr):
    vr = 0.5 * tr / pr
    epsvr = 1e-8
    for _ in range(100):
        f = fun(tr, vr, pr)
        df = (fun(tr, vr + epsvr, pr) - fun(tr, vr - epsvr, pr)) / (2 * epsvr)
        if df == 0:
            raise ValueError("Zero derivative in Duan's method")
        res = f / df
        vr -= res
```

```
        if vr <= 0:
            raise ValueError("Negative molar volume")
        if abs(res) <= 1e-6:
            z = pr * vr / tr
            if z <= 0:
                raise ValueError("Negative compressibility factor")
            return z
    raise RuntimeError("Duan's equation did not converge")

def fug(t, p):
    tr = t / tc
    pr = p / pc
    z = duanz(pr, tr)
    vr = z * tr / pr
    tr2, tr3 = tr**2, tr**3
    vr2, vr4, vr5 = vr**2, vr**4, vr**5
    term1 = (a[0] + a[1]/tr2 + a[2]/tr3) / vr
    term2 = (a[3] + a[4]/tr2 + a[5]/tr3) / (2 * vr2)
    term3 = (a[6] + a[7]/tr2 + a[8]/tr3) / (4 * vr4)
    term4 = (a[9] + a[10]/tr2 + a[11]/tr3) / (5 * vr5)
    term51 = a[12] / (2 * tr3 * a[14])
    term52 = a[13] + 1 - (a[13] + 1 + a[14]/vr2) * np.exp(-a[14]/vr2)
    term5 = term51 * term52
    lnphi = z - 1 - np.log(z) + term1 + term2 + term3 + term4 + term5
    return lnphi

# Standard chemical potential coefficients
coefficients = {
    "c1": 28.9447706, "c2": -0.0354581768, "c3": -4770.67077, "c4": 1.02782768e-5,
    "c5": 33.8126098, "c6": 9.04037140e-3, "c7": -1.14934031e-3, "c8": -0.307405726,
    "c9": -0.0907301486, "c10": 9.32713393e-4, "c11": 0.0
}

def dimensionless_standard_chemical_potential(T, P):
    c = coefficients
    return (c["c1"] + c["c2"]*T + c["c3"]/T + c["c4"]*T**2 +
            c["c5"]/(630 - T) + c["c6"]*P + c["c7"]*P*math.log(T) +
```

```
        c["c8"]*P/T + c["c9"]*P/(630 - T) + c["c10"]*P**2/(630 - T)**2)

def calculate_PH2O(T):
    Tc, Pc = 647.29, 220.85
    c1, c2, c3, c4, c5 = -38.640844, 5.8948420, 59.876516, 26.654627, 10.637097
    t = (T - Tc) / Tc
    return (Pc * T / Tc) * (1 + c1*(-t)**1.9 + c2*t + c3*t**2 + c4*t**3 + c5*t**4)

def calculate_ln_m_CO2(T, P):
    mu0 = dimensionless_standard_chemical_potential(T, P)
    PH2O = calculate_PH2O(T)
    if P <= PH2O:
        raise ValueError("Pressure must exceed water vapor pressure")
    yCO2 = (P - PH2O) / P
    ln_phi_CO2 = fug(T, P)
    return math.log(yCO2 * P) + ln_phi_CO2 - mu0

def calculate_pressure_from_mCO2(T, target_m):
    P = calculate_PH2O(T) + 1
    epsp = 1e-8
    for _ in range(100):
        ln_m = calculate_ln_m_CO2(T, P)
        f = math.exp(ln_m) - target_m
        df = (math.exp(calculate_ln_m_CO2(T, P + epsp)) - math.exp(calculate_ln_m_CO2(T,
P - epsp))) / (2 * epsp)
        P -= f / df
        if abs(f / df) < 1e-6:
            return P
    raise RuntimeError("Pressure iteration failed")

def flash_pressure_duan(T_celsius, Xco):
    T_kelvin = T_celsius + 273.15
    M_CO2 = 44.01  # g/mol
    molality_CO2 = (Xco / (1 - Xco)) * (1000 / M_CO2)  # mol/kg
    P_bar = calculate_pressure_from_mCO2(T_kelvin, molality_CO2)
    return P_bar * 14.5038  # Convert to psia
```

```
# Simulation Parameters
Pwf = 3806.52  # Bottom-hole pressure in psia
T_bh  = 463.5266  # Bottom-hole temperature in Fahrenheit
rw = 0.70833  # Radius of the wellbore in feet
q_t = 1.3662  # Flow rate in ft³/s
d_L = 150  # Segment length in feet
geothermal_gradient = 0.0317  # Geothermal gradient in °F/ft
total_length = 10385  # Total wellbore length in feet
Xco = 0.0425  # CO2 mass fraction in the liquid phase
g = 9.81  # Gravitational acceleration (m/s^2)

alpha = 0.0952
ke = 33.28
c = 0.455
r2 = 0.1080
t = 1
w_m3s = q_t / (24 * 3600 * 35.3147)

td = dimensionless_time(alpha, t, r2)
ft = f_t(td)
A_prime = diffusion_depth(w_m3s, c, ft, ke)

# Initialization for single-phase flow
print("Single-phase flow calculation:")
depth = 0
P = Pwf
T = T_bh
Tei = (T_bh - 32) / 1.8
Ti = Tei
a_geo = geothermal_gradient / 3.28084

flash_point_pressure = None
flash_point_depth = None

# Precompute rho_L_bh and initialize density_prev
T_bh_K = ((T_bh - 32.0) / 1.8) + 273.15
rho_L_bh = liquid_density(T_bh_K)
```

```
density_prev = rho_L_bh

# SINGLE-PHASE FLOW LOOP
while depth < total_length:
    T_K = ((T - 32.0) / 1.8) + 273.15
    density_water = liquid_density(T_K)
    density_avg = (density_prev + density_water) / 2.0
    density_prev = density_water

    v_w = viscosity(T)
    w = 3600.0 * q_t * density_avg
    NR = reynolds(w, rw, v_w)
    f = friction_factor(NR)

    T_celsius = (T - 32) / 1.8
    try:
        Pfp = flash_pressure_duan(T_celsius, Xco)
    except Exception as e:
        print(f'Flash pressure error at {depth:.2f} ft: {e}')
        break

    print(f'Depth: {depth:.2f} ft, T(C): {T_celsius:.2f}, Pfp: {Pfp:.2f} psia, P: {P:.2f} psia')

    if flash_point_pressure is None and P <= Pfp:
        flash_point_pressure = P
        flash_point_depth = depth
        print(f'\n>> Phase transition detected at {depth:.2f} ft, Pfp: {Pfp:.2f} psia <<\n')
        break

    P_new = pressure_drop(P, density_avg, d_L, f, q_t, rw)
    T = temperature_profile_single_phase(Tei, Ti, a_geo, depth / 3.28084, A_prime)

    print(f'Depth: {depth + d_L:.2f} ft, Pressure: {P_new:.2f} psi, Temp: {T:.2f} °C, Density:
{density_avg:.2f} lbm/ft^3')

    depth += d_L
    P = P_new
```

```
if flash_point_depth is None:
    print("\nNo phase transition detected. Assuming single-phase flow throughout.")
    flash_point_depth = total_length

# DOUBLE-PHASE FLOW LOOP
print("\nDouble-phase flow calculation:")
P = flash_point_pressure
depth = flash_point_depth

while depth < total_length:
    T = temperature_profile_double_phase(Tei, Ti, a_geo, depth / 3.28084, A_prime, g, c)
    T_K = ((T - 32.0) / 1.8) + 273.15
    density_water = liquid_density(T_K)
    T_C = T
    density_co2_val = density_co2(P, T_C)

    v_w = viscosity(T)
    T_celsius = T

    try:
        Pfp_calc = flash_pressure_duan(T_celsius, Xco)
    except Exception as e:
        print(f"Flash pressure error at {depth:.2f} ft: {e}")
        break

    XCO2_dynamic = calculate_XCO2(P, T_C)  # Segment-level dynamic CO₂
    X = Xco - XCO2_dynamic

    v_sg = velocity_sg(q_t, rho_L_bh, X, Xco, rw, P, T)
    vm = q_t / (math.pi * rw ** 2)
    vtr = terminal_velocity(density_water, density_co2_val)
    fg = v_sg / (1.2 * vm + vtr)
    fl = 1.0 - fg
    density_curr = fl * density_water + (1.0 - fl) * density_co2_val
    density_avg = (density_prev + density_curr) / 2.0
    density_prev = density_curr
```

```
    print(f"Depth: {depth:.2f} ft, T(C): {T_celsius:.2f}, Pfp_calc: {Pfp_calc:.2f} psia, P: {P:.2f} psia, X: {X:.4f}, f_g: {fg:.4f}")
    print(f"  -> v_sg: {v_sg:.4f}, v_m: {vm:.4f}, v_tr: {vtr:.4f}")

    w = 3600.0 * q_t * density_avg
    f = 0.025
    P_new = pressure_drop(P, density_avg, d_L, f, q_t, rw)

    print(f"Depth: {depth + d_L:.2f} ft, Pressure: {P_new:.2f} psi, Temp: {T:.2f} °C, Density: {density_avg:.2f} lbm/ft^3")

    depth += d_L
    P = P_new

print("\nCalculation complete. Reached wellhead.")
```

CURRICULUM VITAE

Name Surname **:** Force Lugembe NDEGE

EDUCATION **:**

- **B.Sc.** **:** 2020, Dibrugarh University, Faculty of Science and Engineering, Petroleum Engineering Department
- **M.Sc.** **:** 2025, Istanbul Technical University, Mining Faculty, Petroleum and Natural Gas Engineering Department

PROFESSIONAL EXPERIENCE AND REWARDS:

- 2016-2020: Indian government scholarship (ICCR) beneficiary.
- 2021-2025: Presidency for Turks Abroad and Related Communities (YTB) scholarship beneficiary
- 2023- current: Internation business development office at ACIBADEM Healthcare Group